USGS
science for a changing world

Subsurface, High-Resolution, Seismic Images from Cherry Valley, San Bernardino County, California: Implications for Water Resources and Earthquake Hazards

by

R. D. Catchings, G. Gandhok, M. R. Goldman, E. Horta, M. J. Rymer, P. Martin, and A. Christensen

Open-File Report 99-26

1999

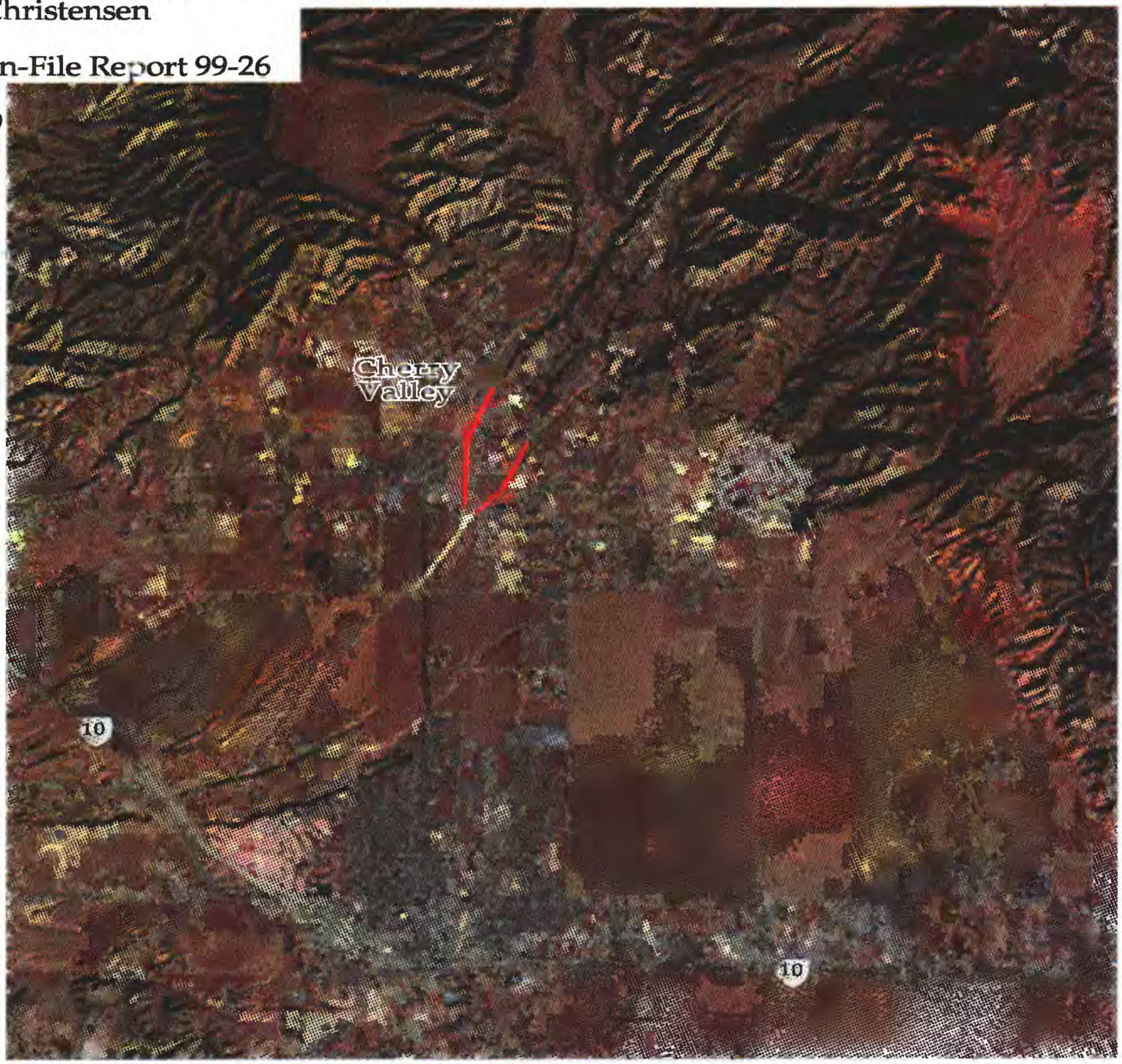

U. S. DEPARTMENT OF THE INTERIOR
U.S. GEOLOGICAL SURVEY

Menlo Park, California

Table of Contents

List of Tables

List of Figures

Introduction

Cherry Valley is located within San Gorgonio Pass, approximately 150 km (93 miles) east of Los Angeles, California. Because of its arid environment and its proximity to the San Andreas fault system, the area is important from both water-resources and earthquake-hazards perspectives. In this report, we present seismic imaging data and interpretations of subsurface structures that are useful for groundwater-resource and earthquake hazard evaluation in the Cherry Valley area (Fig. 1).

Groundwater is the major source of water supply in San Gorgonio Pass. Pumping since the early 1900's has resulted in groundwater-level declines of more than 100 ft in some parts of the area that are monitored by the San Gorgonio Pass Water Agency (SGPWA). To meet the growing demand for water, the SGPWA contracted with the California Department of Water Resources (DWR) to purchase water from the State Water Project (SWP). The SGPWA has completed several studies to determine the feasibility of artificially recharging SWP water and local water by surface spreading (Boyle Engineering Corporation, 1991 and 1992). As a result of these studies, a potential artificial recharge site was selected in the Cherry Valley area along Little San Gorgonio Creek, south of the Banning fault (Fig. 1). The subsurface material at the recharge site is composed of coarse-grained alluvial deposits interbedded with low-permeability, fine-grained deposits (Boyle Engineering Corporation, 1992). If the fine-grained deposits are laterally extensive, these deposits may significantly impede the downward movement of the recharge water and cause the recharge water to become perched. Additional investigation is necessary to determine the lateral extent of the fine-grained deposits. The proposed recharge site is south of the Banning fault, and there may be other unidentified faults in the subsurface. Because faults act as barriers to groundwater flow in most alluvial systems, knowledge of such faults could be particularly valuable in the vicinity of the proposed recharge site.

The San Gorgonio Pass area is seismically active (Magistrale and Sanders, 1996), and numerous surface faults have been mapped in the area (Matti et al., 1992). Because of their proximity to the San Andreas fault system, Cherry Valley and other nearby desert communities are susceptible to strong shaking generated by large-magnitude earthquakes. Some of these communities, however, may also be susceptible to strong shaking generated by smaller active faults located beneath them. Such faults may be concealed at the surface by alluvium within the valleys. The seismic hazard posed to these communities would be greatly increased by the presence of such "blind faults", as was found for the 1994 Mw 6.7 Northridge earthquake (Hauksson et al, 1995). Studies have found that unconsolidated (low-velocity) sediments can amplify shaking generated by earthquakes (Borcherdt and Glassmoyer, 1994). The location and velocity structure of faults related to blind-fault systems has been successfully identified with seismic imaging methods (Catchings et al., 1998). Knowledge of such faults aid in seismic hazard

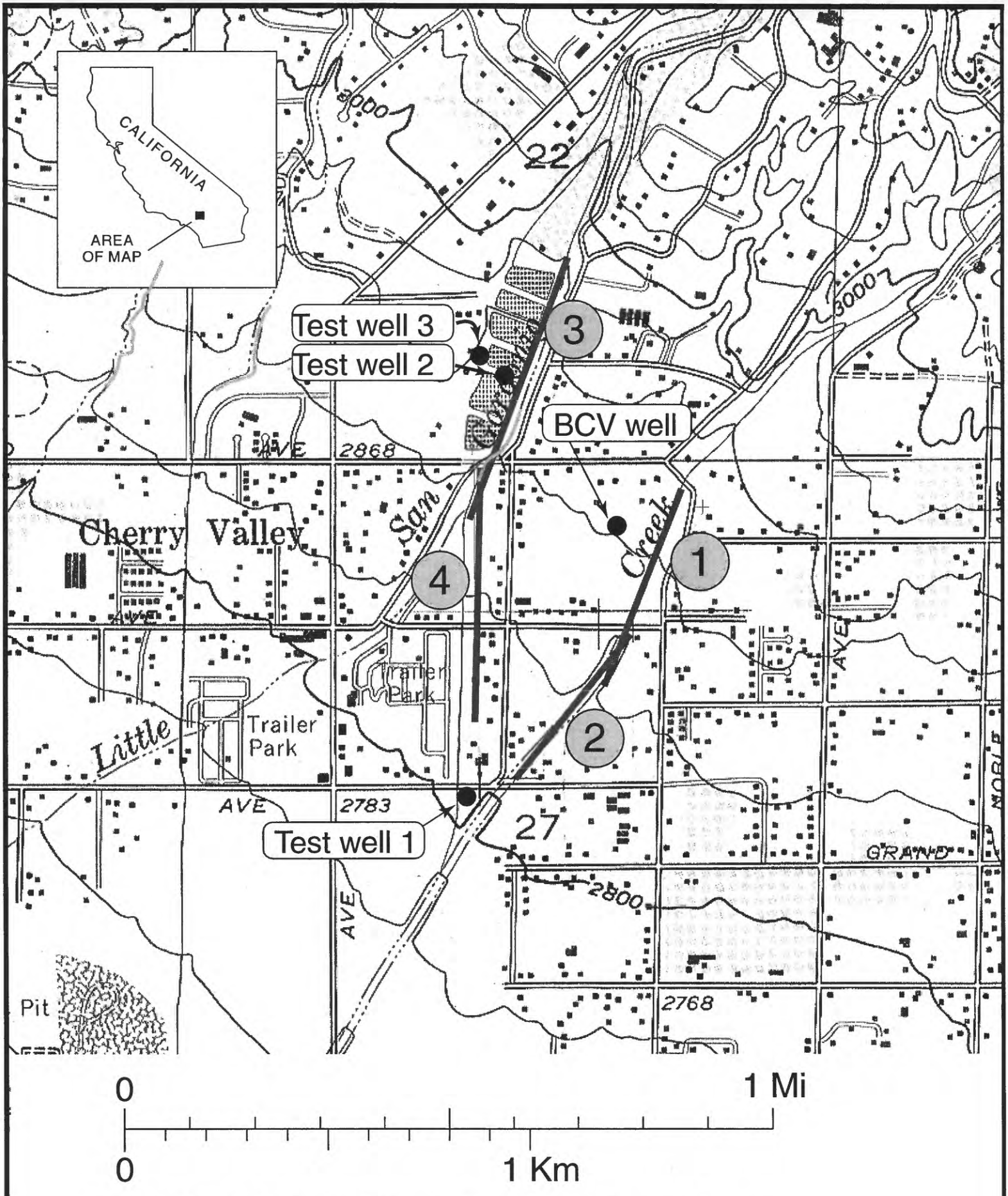

Fig. 1 Map of Cherry Valley with seismic lines and wells.

assessment and mitigation.

The objectives of this study were to: (1) determine lateral variations in the stratigraphy of the proposed recharge site in Cherry Valley, (2) locate faults that act as barriers to groundwater flow and that may pose seismic hazards to the surrounding communities, and (3) measure the velocity and geometry of shallow sediments that may amplify seismic waves during large earthquakes. Four high-resolution seismic reflection and refraction profiles were acquired along Little San Gorgonio and Noble Creeks in the Cherry Valley area (Fig. 1), and the resulting seismic images were compared to well logs from nearby boreholes.

Local Geology and Tectonics

The local, near-surface geology in the Cherry Valley area consists of Pliocene sandstones, gravels, and clays that are overlain by Quaternary alluvium. The alluvium is derived from Precambrian metamorphic and igneous rocks (gneisses, schists, and Mesozoic granites) from the adjacent San Bernardino mountains (Jennings et al., 1977). On the basis of borehole cuttings in the Cherry Valley area, the upper 300 m consists of Pliocene and Quaternary sediments that can be grouped into four lithologic units, the San Timoteo Formation, the Old Red Gravel, an Older Alluvium unit, and a Quaternary Alluvium unit (Boyle Engineering Co. Director, 1992). The San Timoteo Formation, the oldest geologic unit encountered in the test wells at the proposed recharge site, is located at 75 to 100 m (~246 to 330 ft) below ground surface (bgs). The San Timoteo Formation consists of poorly sorted-to-well-sorted, partly consolidated, fine-to-coarse sand, gravel, and cobbles with thin clay layers. The Old Red Gravel unit overlies the San Timoteo Formation and consists of about 30 m of reddish-brown, poorly sorted, coarse gravel, sands, and silt. The Older Alluvium unit overlies the Old Red Gravel and consists of poorly sorted, unconsolidated gravel, sands, cobbles, and boulders. The Quaternary Alluvium unit is generally located within the upper 18 m (~60 ft) and consists of silt, fine and coarse sands, gravels, and granite boulders. The depth of the water table varies laterally, but in most wells, it was found to be within the San Timoteo Formation (Boyle Engineering Co. Director, 1992). However, perched water tables were also found at stratigraphically higher levels (~50 to 60 m - ~165 to ~200 ft).

The San Andreas fault is located approximately 19 km (12 miles) north of Cherry Valley, within the San Bernardino mountains. A series of active right-lateral, strike-slip faults, wrench faults, and thrust faults are believed to extend across the Cherry Valley region (Matti et al., 1992). Three of the known larger faults in the Cherry Valley area are the Banning fault on the northern edge of the valley and the Claremont and the San Jacinto faults on the southern end of the valley. These faults, other faults farther north, and possibly other unknown faults beneath the valley comprise the San Andreas fault system in the San Gorgonio Pass Region.

Seismic Survey

Data Acquisition

In August 1997, the U. S. Geological Survey acquired four high-resolution seismic reflection and refraction profiles along Little San Gorgonio and Noble Creeks in Cherry Valley (Fig. 1). The seismic profiles (labeled CV-1 through CV-4 in Fig. 1) ranged in length from approximately 400 m to 700 m (see Table 1), and three of the four profiles were oriented in a northeast-southwest direction. A fourth profile was oriented approximately north-south.

Approximately 4 seconds of data were recorded using a linear array of Geometrics Strataview RX 60™ seismographs, each with 60 active channels. Two to four seismographs were used along each of the profiles, with a total of 120 to 240 active channels. The data were stored on the computer hard drive of the seismographs during acquisition in the field and was later downloaded to 4-mm tape for permanent storage in SEG-Y format.

We used 40-Hz, single-element, Mark Products L-40A™ geophones spaced at either 2.5 or 3 m along each of the profiles. Seismic sources (shots), located at a depth of about 0.5 m, were laterally spaced approximately every 5 or 6 m and were co-located (1-m lateral offset) with the geophones along the profiles. The shots were generated by a BETSY™ Seisgun using 8-gauge shotgun blanks. Shot timing was determined electronically at the seismic source when the hammer electrically closed contact with the BETSY™ Seisgun, sending an electrical signal to the seismograph.

Prior to acquiring the data, each recording site and shotpoint was measured with a meter tape and flagged to obtain the proper spacing. After the seismic data were acquired, we used an electronic distance meter (EDM), with theoretical accuracies of approximately 0.001 m, to measure the recording sites and shotpoint locations (see Appendices A and B).

Table 1. Acquisition parameters for Cherry Valley seismic profiles. Distances are relative to first shotpoint.

Profile #	Orientation	Length of Geophone Profile (m)	Length of Shotpoint Profile (m)	No. of Shots	No. of (CDP)	Maximum Fold
1	NE-SW	441.75	548.89	101	398	84
2	NE-SW	297.13	424.76	80	290	58
3	NE-SW	590.69	688.53	133	514	113
4	N-S	539.70	644.19	101	396	87

Shot and Geophone Locations

Variations in shotpoint and geophone locations and elevations can cause difficulty in stacking the reflection data and in accurately measuring velocities if these variations are not taken into account in processing the data. Large variations in the line geometry may also result in data artifacts that are interpreted as structure. Therefore, the line geometries are presented (see Appendices A-E) for anyone who may wish to reprocess or reinterpret the data. To correlate variations in seismic velocities and seismic images with possible geometrical variations, graphical displays of the geometry along each profile are presented in this report. These displays include shotpoint and geophone elevations, lateral variations from straight lines of shotpoint and geophone arrays, and fold (described below). In many instances, abrupt changes in elevation can be correlated with faults or major changes in stratigraphy, but apparent faults or stratigraphic changes that correlate with significant or abrupt deviations of shotpoint and geophone arrays from a straight line are likely to be artifacts of geometry. Areas of low fold or abrupt changes in fold may also contribute to the appearance of artifacts in the seismic data.

Seismic Data Processing

Both reflection and refraction data were available because we acquired the seismic data using a shoot-through configuration. This type of data acquisition has numerous advantages over conventional seismic data acquisition because detailed velocity data are available and fold is typically much greater over most of the array.

Seismic Refraction Velocity Analysis

We used two types of seismic data processing, refraction analysis and reflection processing. In refraction data processing, we used a seismic tomographic inversion method developed by Hole (1992), whereby, first arrivals on each seismic trace were used to measure detailed velocities from depths ranging from about one meter below the surface to depths as great as 150 m. For greater depths, velocities needed in seismic reflection stacking were determined using semblance, parabolic methods, or apriori knowledge of the local geology. As described below, we used the velocities derived from these methods to convert the time-images to depth-images and, where necessary, to migrate the seismic reflection images.

Seismic Reflection Processing

Seismic reflection data processing was accomplished on a Sun Sparc 20 ™ computer using an interactive seismic processing package known as ProMAX™. The following steps were involved in data processing:

Geometry Installation

Lateral distances and elevations, described above, were used to define the geometrical set up of each profile. We installed the electronically-measured geometries into the ProMAX™ processing package for each

profile separately so that shot and receiver elevations and locations could be used in the processing routine.

Trace Editing

Occasionally, bad coupling between the geophones and the ground, malfunctioning geophones, or cultural noise close to the seismic receivers resulted in unusually noisy traces at those locations. Traces representing those locations were edited. However, such traces were not always unsuitable for each shot gather; therefore, independent trace editing was employed for each shot gather.

Bandpass Filtering

Most of the data of interest for seismic imaging and velocity measurement are well above 25 Hz, and most of the undesirable seismic data, such as surface waves and shear waves, were well below 25 Hz. Therefore, a bandpass filter with a low cut of 25 Hz was used to remove most surface and shear waves, as well as cultural noise.

F-K Filtering

Not all surface waves were removed by simple bandpass filtering. To remove the remaining surface waves and air waves, we used an F-K filter.

Timing Corrections

Although the shotgun source electronically triggers the seismographs, there are small (~2 ms) delays between the electrical trigger and the actual shotgun blasts. We corrected for the delays by removing a constant 2 ms from the start time of each shotgather.

Velocity Analysis

Velocities in the shallow section (~1 m to ~150 m) were determined using velocity inversion techniques on first arrivals, but velocities in the deeper section were determined using shotgathers (fitting hyperbolae) and CDP stacks (semblance).

Elevation Statics

Elevation statics were also employed to correct for variations in elevations using the electronically-determined locations and velocities derived from the refraction velocity analysis.

Moveout Correction

Due to progressively greater traveltimes for the seismic waves to reach sensors that were progressively farther from each shotpoint, there was a delay (moveout) for each seismic arrival on the seismic record. To sum (stack) the data at each common depth point (CDP), a correction was made for the moveout using velocities obtained from the velocity analysis.

Muting

To remove refractions and other arrivals that were not completely removed using filtering techniques, we used trace muting before and after stacking.

Stacking

To enhance the seismic signal at each location, individual reflections

were summed together in a process called stacking.

Depth Conversion

For stacked seismic reflection sections that were not migrated, we converted the time sections to depth sections using RMS velocities converted from the velocity analysis described in the velocity section.

Migration

Due to the presence of numerous faults and diffraction points in the subsurface, diffraction hyperbolae were observed throughout the section. We used pre-stack migration to collapse the diffraction hyperbolae to better identify the major faults. Migration is a mathematical process that moves seismic energy (such as diffractions) back to their correct position in the subsurface.

Seismic Data

Profile CV-1

Profile CV-1 trended approximately N32°E along Noble Creek between Orchard Avenue and Vineland Avenue (Fig. 1). Three RX-60 seismographs with 180 live channels were used to record approximately 101 shots along the 549-m-long profile. Due to cultural features (roads, utility lines, etc), two shotpoints were skipped.

Elevations were highest on the northeastern end of the profile and decreased to the southwest along the alluvial fan. Geophone elevations decreased by about 16 m from northeast to southwest (Fig. 2), and their locations varied from a straight line connecting the endpoints by less than 1.5 m over the approximately 500-m-long geophone array (Fig. 3). The minor variation in linearity of the geophone array suggests that line geometry is unlikely to cause significant artifacts in the data that can be confused with structure. Similarly, most shotpoint elevations varied by less than 20 m (Fig. 4), and their locations varied by less than 1.5 m from a straight-line array (Fig. 5). Fold (the theoretical number of times a reflection point at a given location is sampled) along CV-1 was relatively smoothly varying because of the stationary recording array. Maximum folds of approximately 84 were obtained near the center of the array but decreased to approximately 1 near the ends of the recording array (Fig. 6). This variation in fold suggests that the most reliable reflection images are near the center of the array. In practice, however, we've found that folds above about 30 are highly reliable for the upper 300 m when using a BETSY Seisgun ™.

Profile CV-2

Profile CV-2 trended approximately N47°E along Noble Creek between Vineland Avenue and Cherry Valley Boulevard and was located southwest of CV-1. CV-1 and CV-2 overlapped by about 75 m near their intersection (Fig. 1). The seismic data for CV-2 was recorded on two RX-60 seismographs

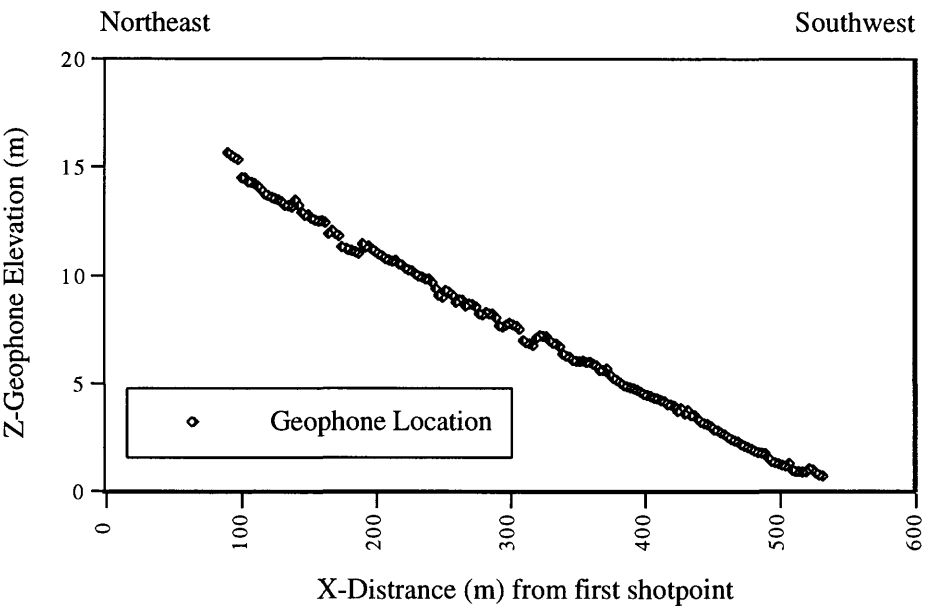

Figure 2. Geophone elevation along Line 1. Elevation is relative to the topographically lowest shotpoint along the line.

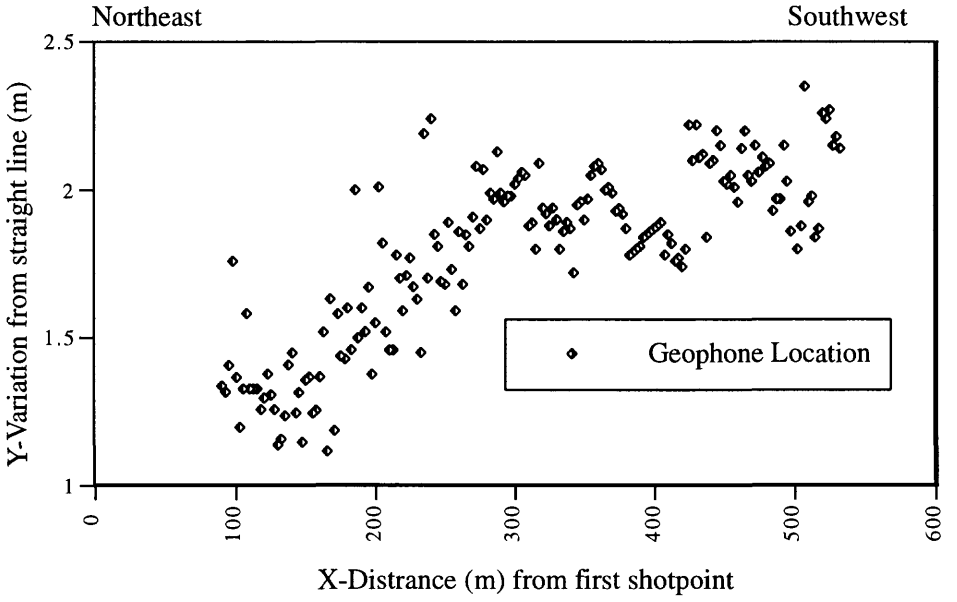

Figure 3. Geophone variation from a straight line connecting the first and last geophone in Line 1.

Line 1

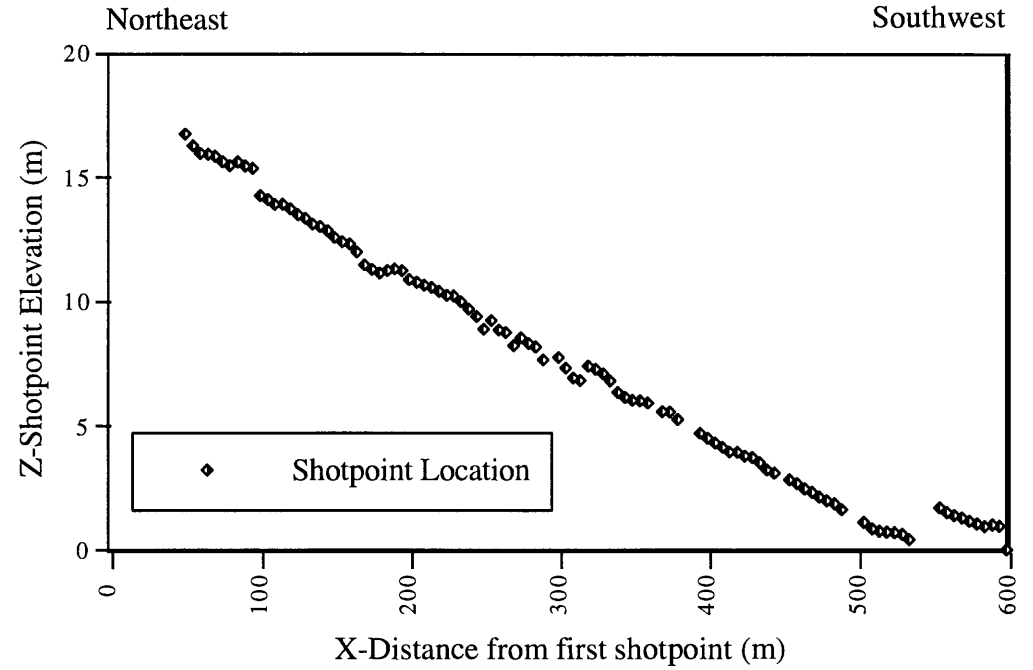

Figure 4. Shotpoint elevation along Line1. Elevation is relative to the topographically lowest shotpoint along the line.

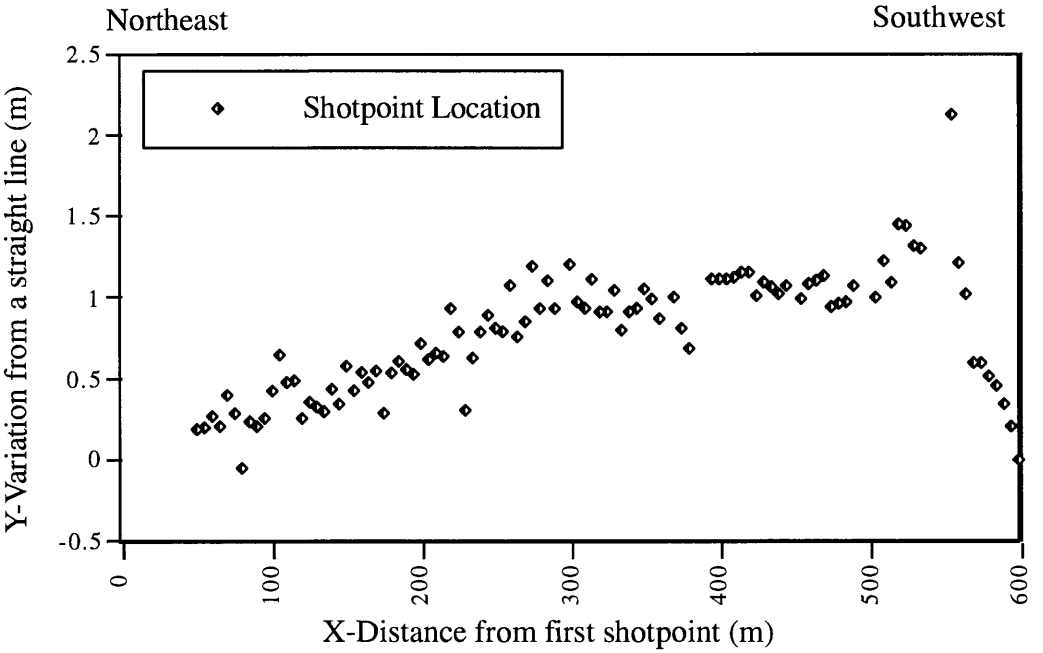

Figure 5. Shotpoint variation from a straight line connecting the first and last shotpoint in Line1.

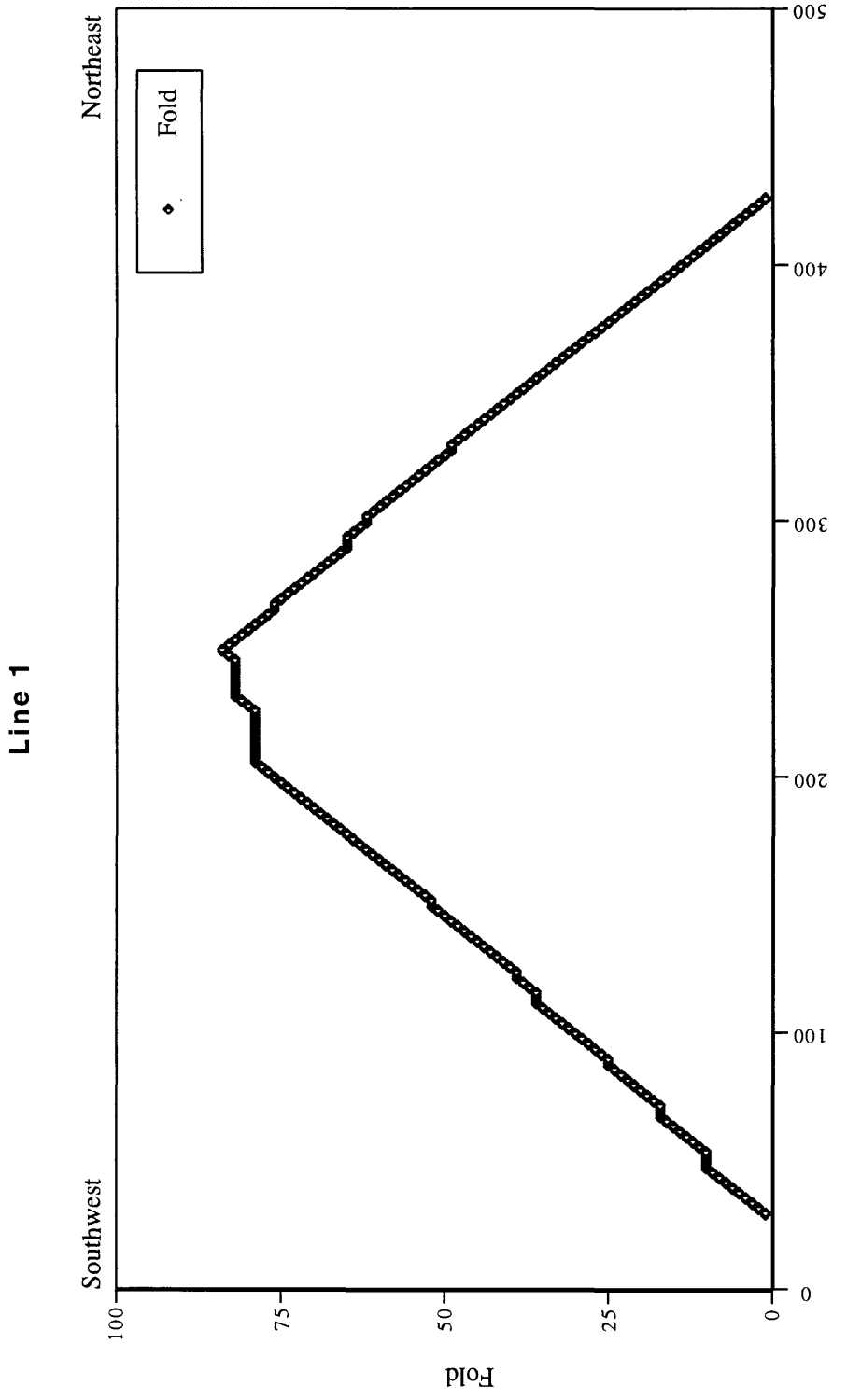

Figure 6. Fold as a function of common depth points along Line 1. Distance is relative to southwesternmost shotpoint.

with 120 live channels. A total of eighty shots were recorded along the ~425-m-long profile. Due to cultural features (roads, utility lines, etc), some shotpoints were skipped.

In general, elevation decreased from northeast to southwest, with the higher elevations on the northeastern end of the profile. Geophone elevations decreased by about 11 m from northeast to southwest (Fig. 7), and individual geophone locations varied from a straight line by less than 1.0 m over the approximately ~425-m-long array (Fig. 8). Similarly, shotpoint elevations varied by less than 15 m (Fig. 9), and shotpoint locations by less than 1.0 m from a straight-line array (Fig.10). Fold along CV-2 was relatively smoothly varying because of the stationary recording array. Maximum folds of approximately 58 were obtained near the center of the array but decreased to approximately 1 near the ends of the recording array (Fig. 11).

Profile CV-3

Profile CV-3 was located along Little San Gorgonio Creek, with most of the profile north of Orchard Avenue. The profile was adjacent to five recharge ponds constructed by the San Gorgonio Water District, and the profile crossed from the northwest side of Little San Gorgonio Creek to the southeast side at Orchard Avenue. CV-3 trended subparallel (N30°E) to CV-1 and was located approximately 400 m northwest of CV-1 at the closest point between the two profiles.

We used four RX-60 seismographs with 240 live channels to record approximately 133 shots along the ~425-m-long profile. As with CV-1, elevation decreased from northeast to southwest, with the higher elevations on the northeastern end of the profile. Geophone elevations decreased by more than 30 m from northeast to southwest (Fig. 12), and individual geophone locations varied from a straight line by about 1.5 m over the approximately ~591-m-long geophone array (Fig. 13). Similarly, shotpoint elevations varied by more than 30 m (Fig. 14), and locations varied by less than 2.0 m from a straight-line over the approximately 689-m-long shotpoint array (Fig. 15). Fold along CV-3 was relatively smoothly varying because of the stationary recording array. Maximum folds of approximately 113 were obtained near the center of the array, but decreased to approximately 1 near the ends of the recording array (Fig. 16).

Profile CV-4

Profile CV-4 trended approximately north-south along the present route of Little San Gorgonio Creek (Fig. 1). CV-4 trended from Orchard Avenue to about one-half block north of Cherry Valley Boulevard, where it overlapped CV-3 by about 75 m. Both profiles cross the concrete lining of Little San Gorgonio Creek.

The seismic data for CV-4 was recorded on three RX-60 seismographs with 180 live channels. A total of eighty shots were recorded along the ~540-

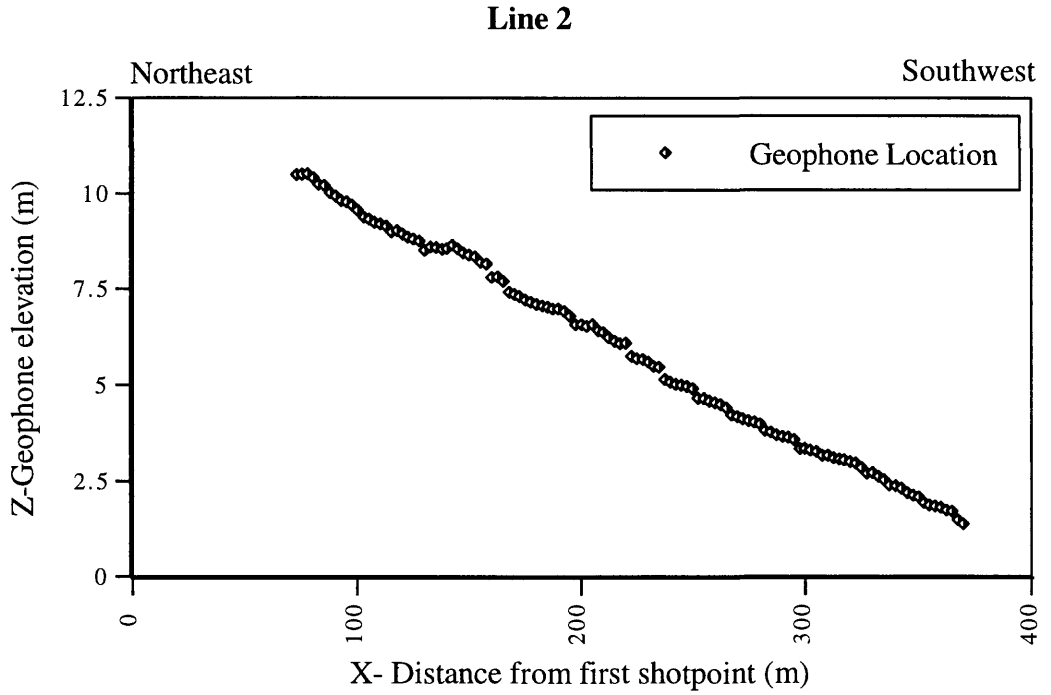

Fig. 7. Geophone elevation along Line 2. Elevation is relative to the topographically lowest shotpoint along Line 2.

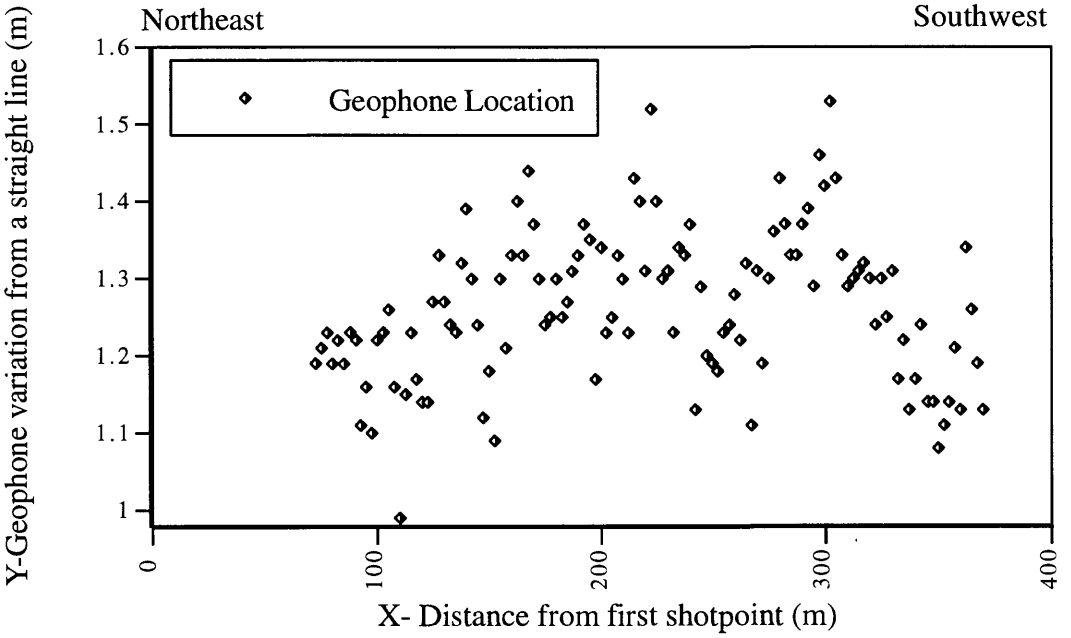

Fig. 8. Geophone variation from a straight line connecting the first and last geophone of Line 2. Distance is relative to the southwesternmost shotpoint.

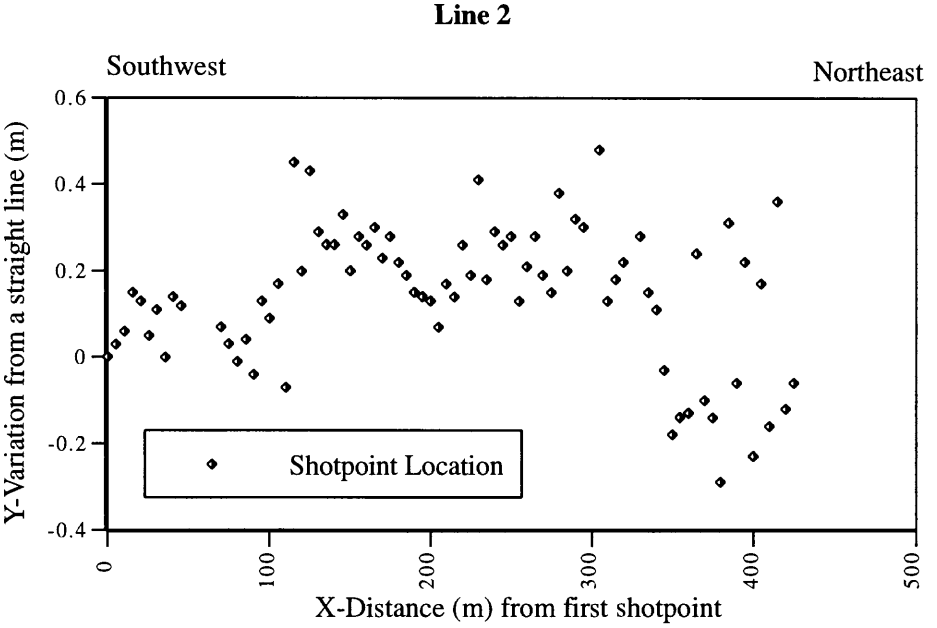

Fig. 9. Shotpoint variation from a straight line connecting the first and last shotpoint of Line 2.

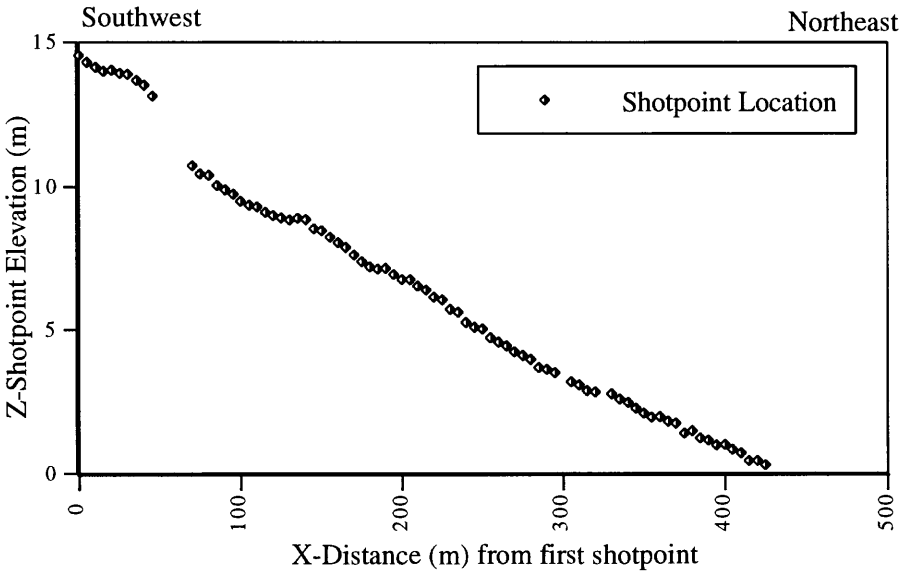

Fig. 10. Shotpoint elevation in Line 2. Elevation is relative to the topographically lowest shotpoint.

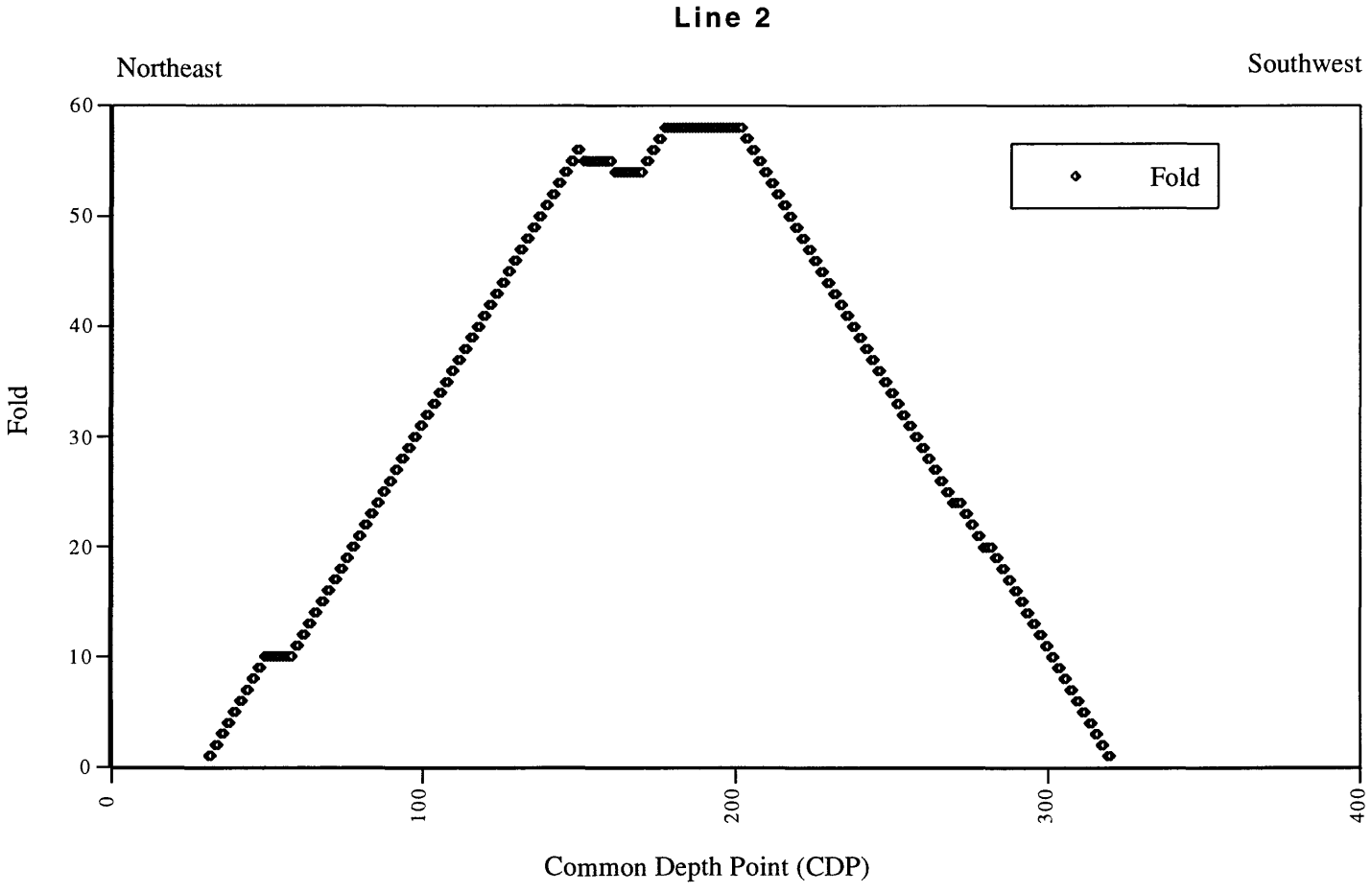

Fig. 11. Fold as a function of Common Depth Point (CDP) along Line 2.

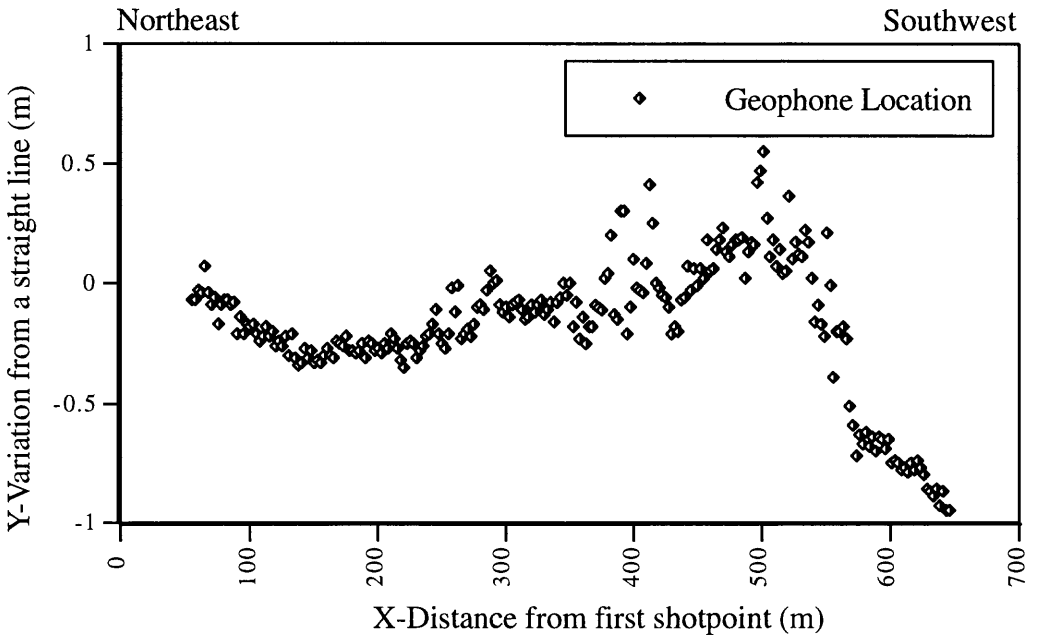

Figure 12. Geophone variation from a straight line connecting the first and last geophone along Line 3.

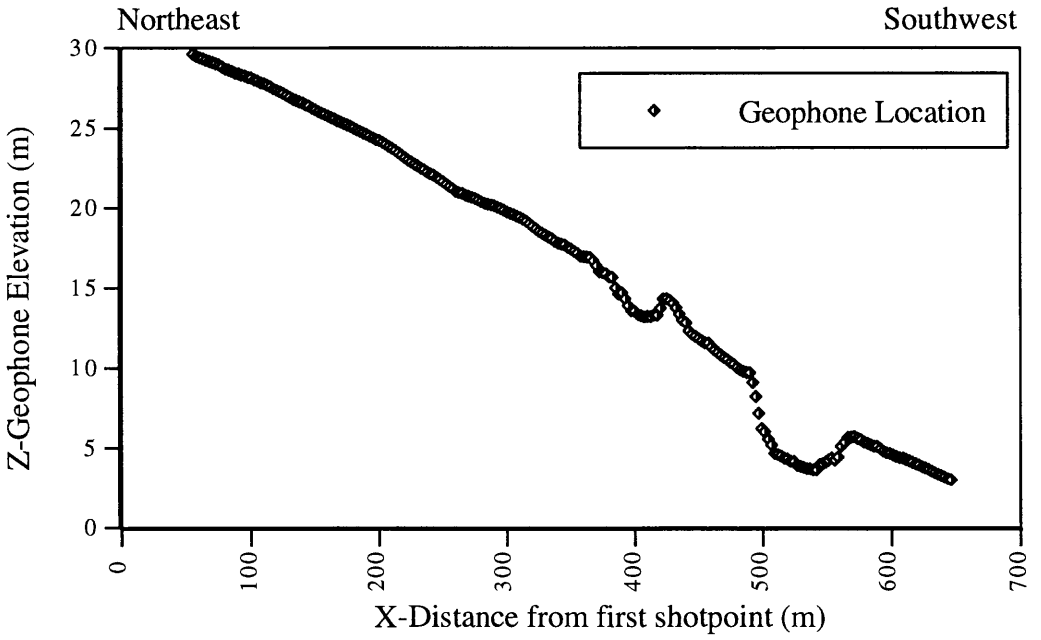

Figure 13. Geophone elevation along Line 3. Elevation is relative to the topographically lowest shotpoint.

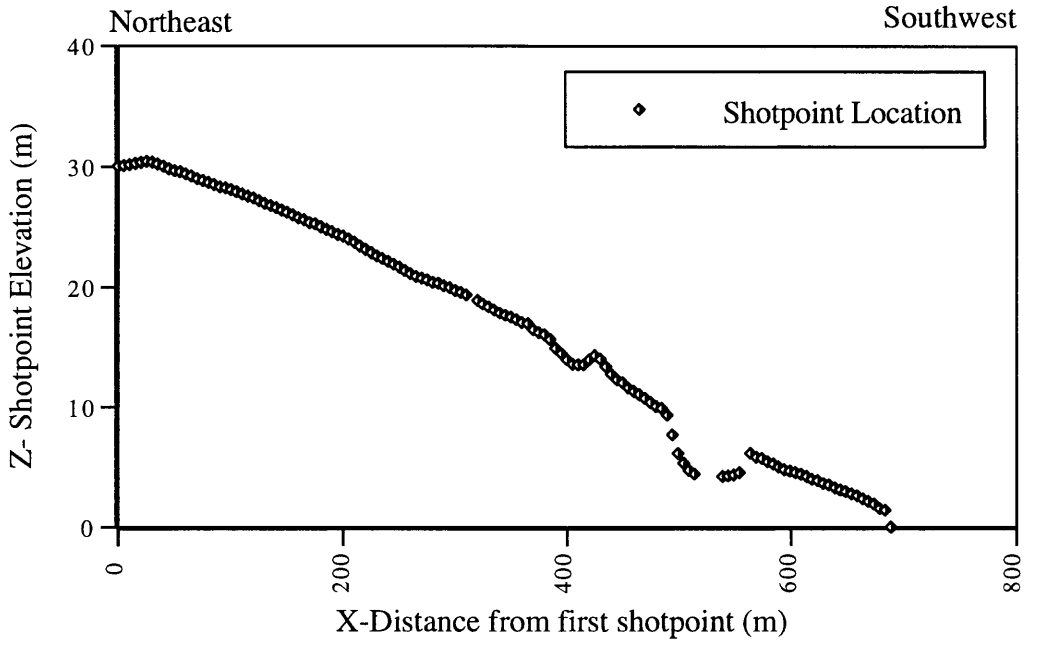

Fig.14. Shotpoint elevation is relative to the topographically lowest shotpoint along Line 3.

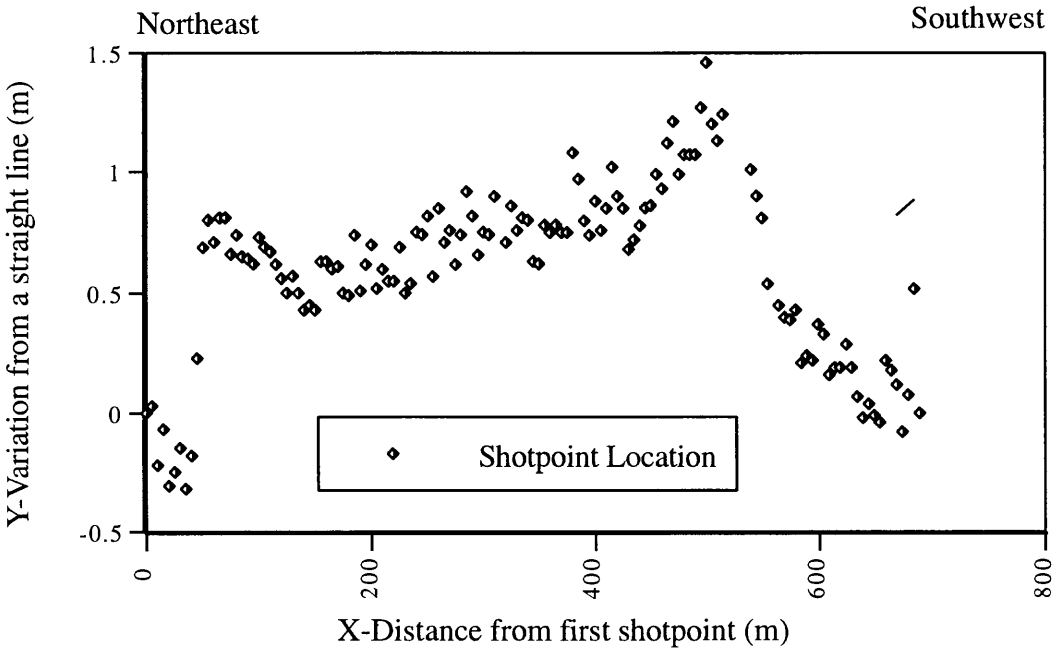

Fig.15. Shotpoint variation from a straight line connecting the first and last shotpoint along Line 3.

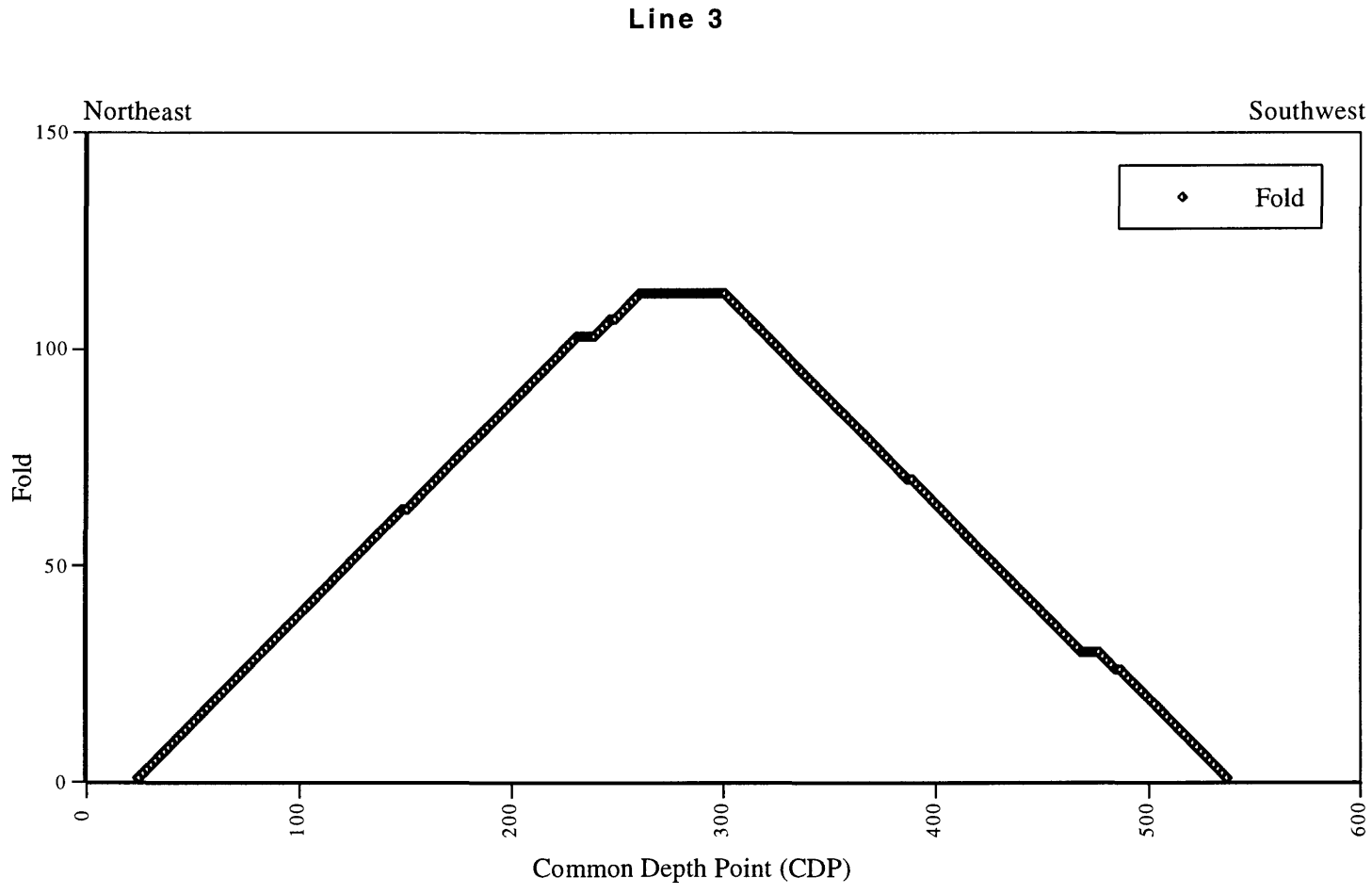

Fig.16. Fold as function of Common Depth Point (CDP) along Line 3. Distance is relative to the northeasternmost shotpoint along Line 3.

m-long geophone array. Elevations decreased from northeast to southwest, with the higher elevations on the northeastern end of the profile. Geophone elevations decreased by about 17 m from northeast to southwest (Fig. 17), and individual geophone locations varied from a straight line by about 2.5 m over the approximately ~540-m-long array (Fig. 18). Similarly, shotpoint elevations varied by about 20 m (Fig. 19,) and individual locations varied by about 2.5 m from a straight-line over the ~644 m of shotpoint array (Fig. 20).

Along CV-4, maximum folds of approximately 87 were obtained near the center of the array, but decreased to approximately 1 near the ends of the recording array (Fig. 21).

Interpretation

Profiles CV-1 and CV-2

Interpreted Reflection Section

Stacked, migrated, and interpreted seismic reflection images of the upper 300 m (~1000 ft) along profiles CV-1 and CV-2 are shown in figures 22 and 23. Profiles CV-1 and CV-2 were acquired separately, but they have been joined where the two profiles cross. Because CV-2 overlapped CV-1 by more than 75 m, it is possible to make correlations between reflections from each line. Both seismic profiles crossed artificial fill and the concrete lining along Noble Creek, causing a velocity pull-up effect, whereby, reflectors appear closer to the surface. A different datum was used for CV-2 than for CV-1, as each line uses a datum relative to its topographically lowest shotpoint.

These data show numerous reflectors from the near-surface to depths of approximately 300 m. These reflectors can be correlated with principal lithologic units, as defined from borehole samples by Boyle Engineering Corporation (1992) (Fig. 23). By correlating specific reflectors with specific lithologic units, lateral variations in the depths and continuity of these lithologic units can be observed. Most reflectors are continuous across profiles CV-1 and CV-2, but depths to these reflectors vary laterally. We interpret faults where a series of reflectors are abruptly and vertically offset over a range of depths. Vertical offsets range from a few meters to several tens of meters. Of particular interest to this study are those faults that appear to significantly offset the water table and those that reach the surface.

Significant offsets of the apparent water table reflector are observed near meter 175 and between meters 300 and 500 along CV-1. At meter 175, all principal lithologic units, including the water table, appear to have been vertically offset along a principal fault. However, between meters 300 and 500, there appear to be a series of faults that have cumulatively offset the water table by as much as 50 m. If our interpretation is correct, it suggests that the lateral flow of water from the northwest to the southeast would be disrupted at depths above 150 m.

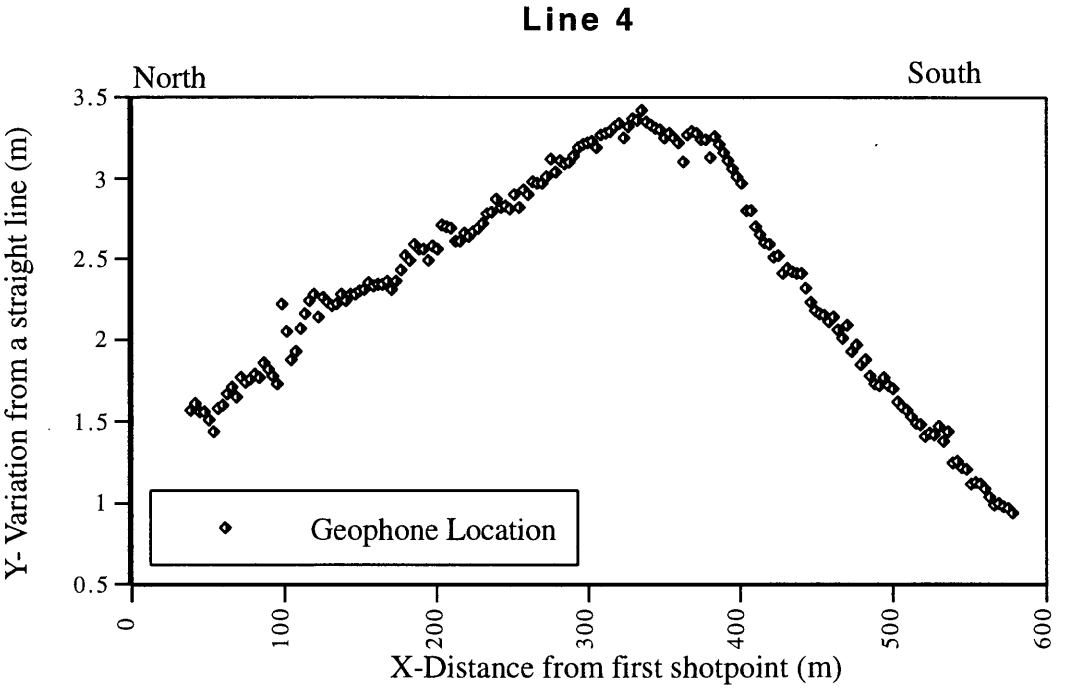

Fig.17. Geophone variation from a straight line connecting the first and last geophone along Line 4.

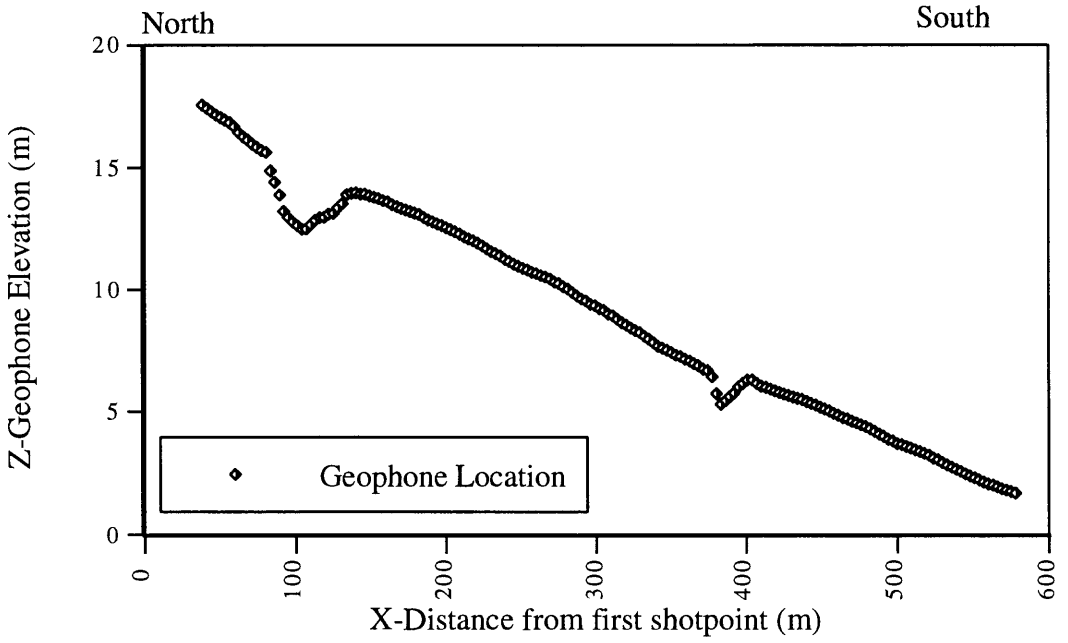

Fig.18. Geophone elevation along Line 4. Elevation is relative to the topographically lowest shotpoint.

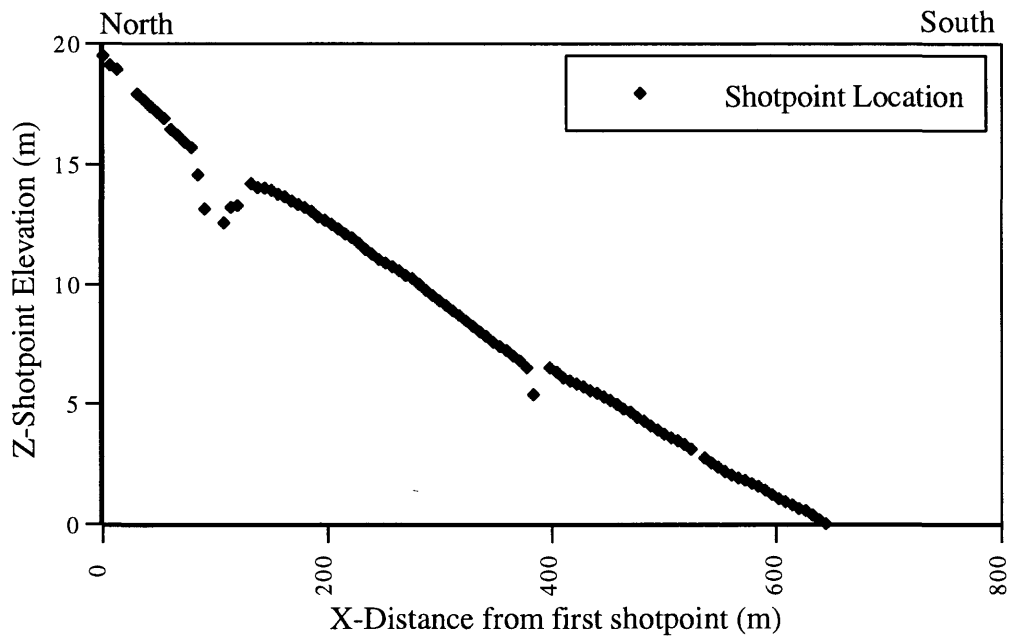

Fig. 19 Shotpoint elevation along Line 4. Elevation is relative to the topographically lowest shotpoint along Line 4.

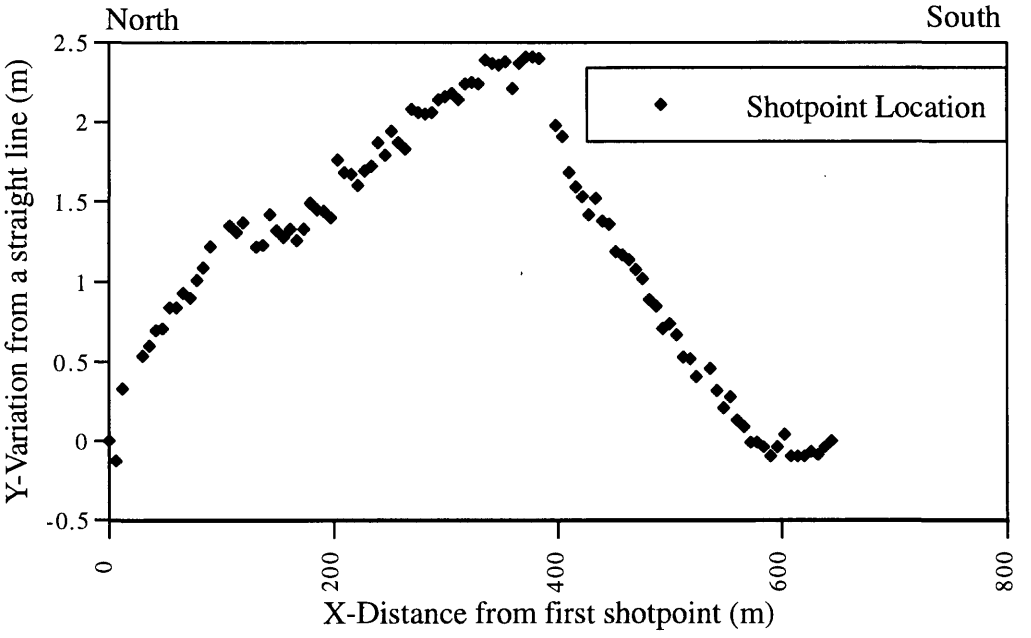

Fig.20. Shotpoint variation from a straight line connecting the first and last shotpoint in Line 4.

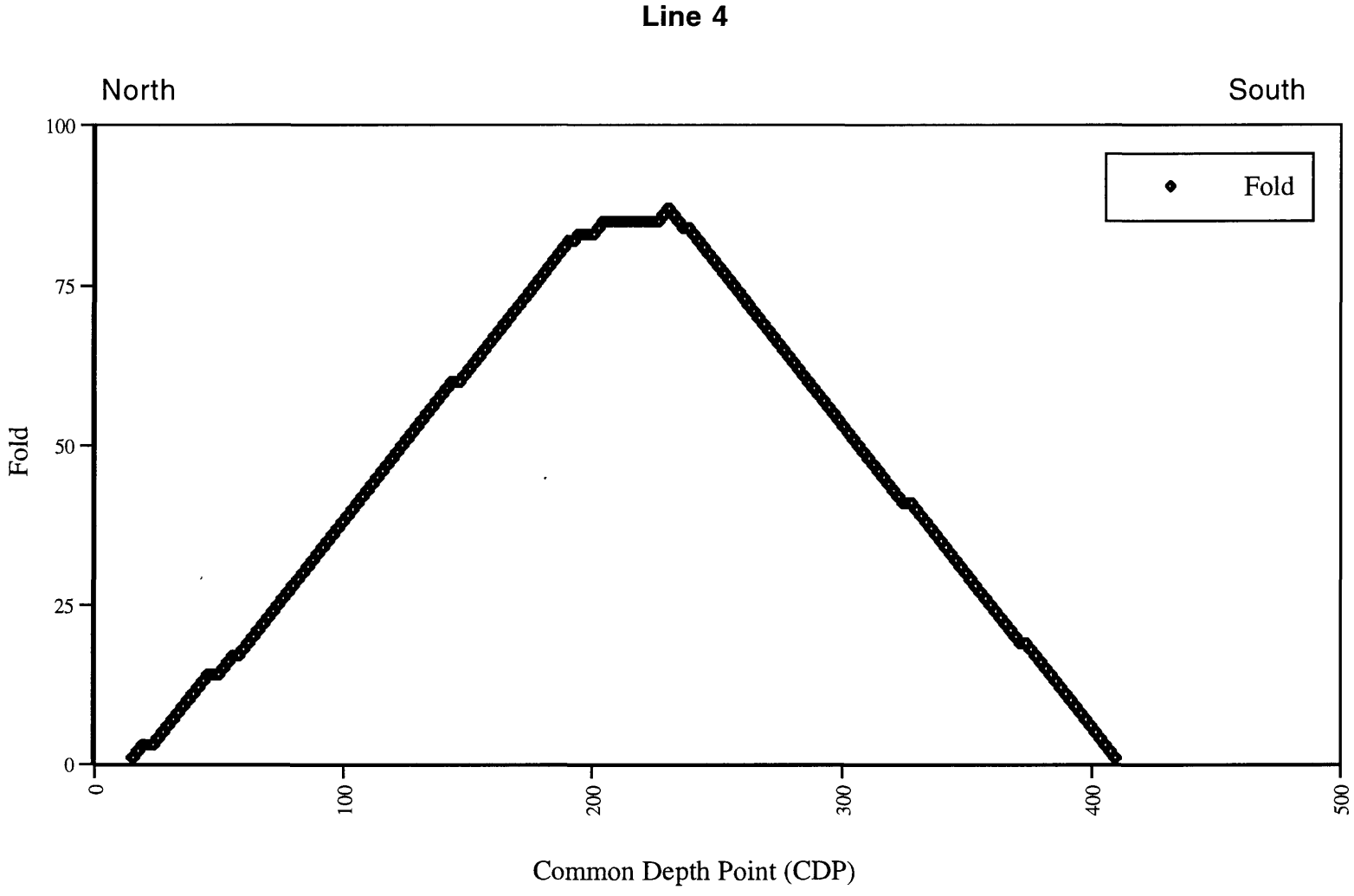

Fig.21. Fold as a function of Common Depth Point CDP) along Line 4.

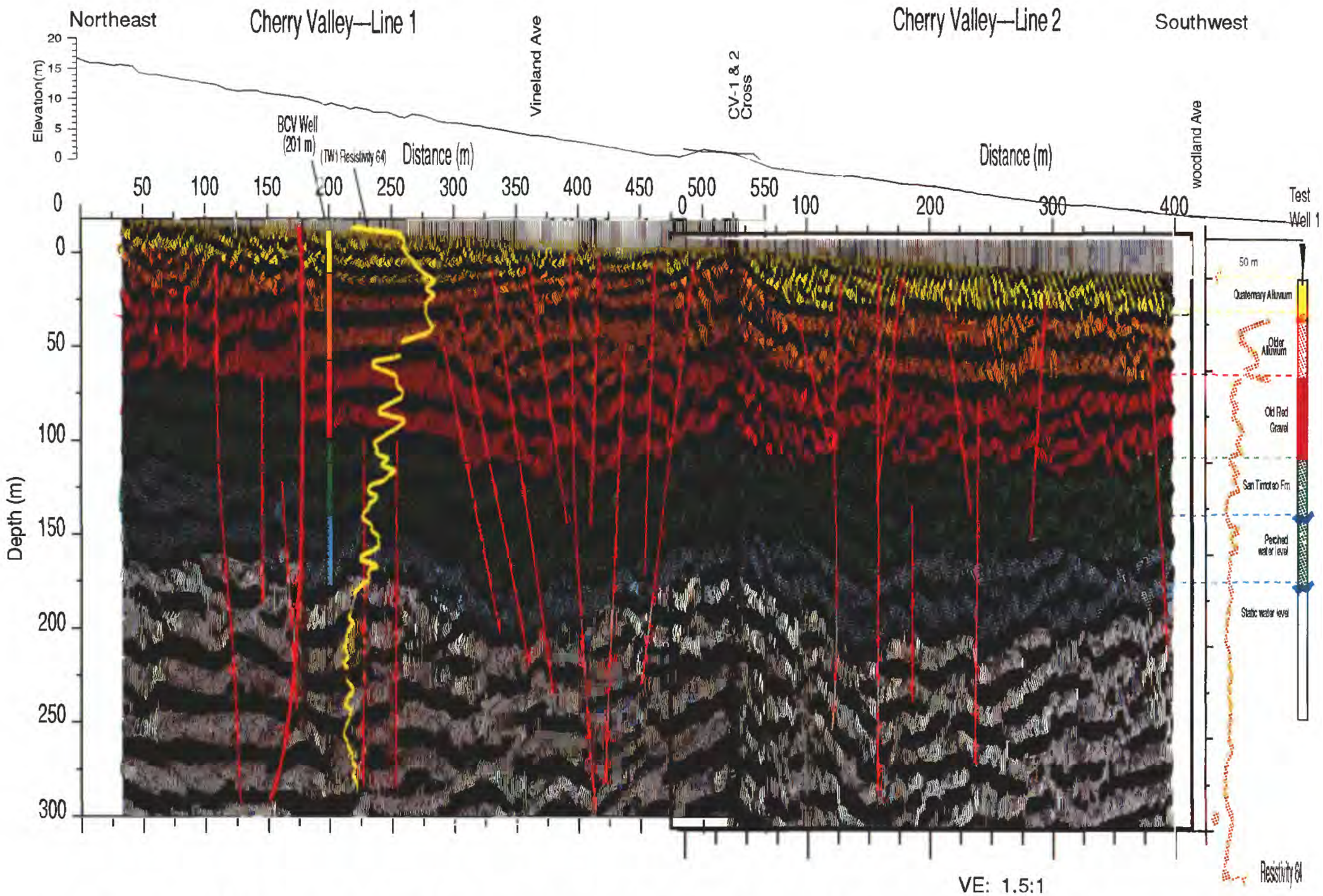

Fig. 23. Migrated and interpreted seismic reflection images along lines 1 and 2 with the BCV and Test Well 1 wells. Colors denote stratigraphic units described in the text. Interpreted faults are shown as red lines. Resistivity profiles are shown in yellow.

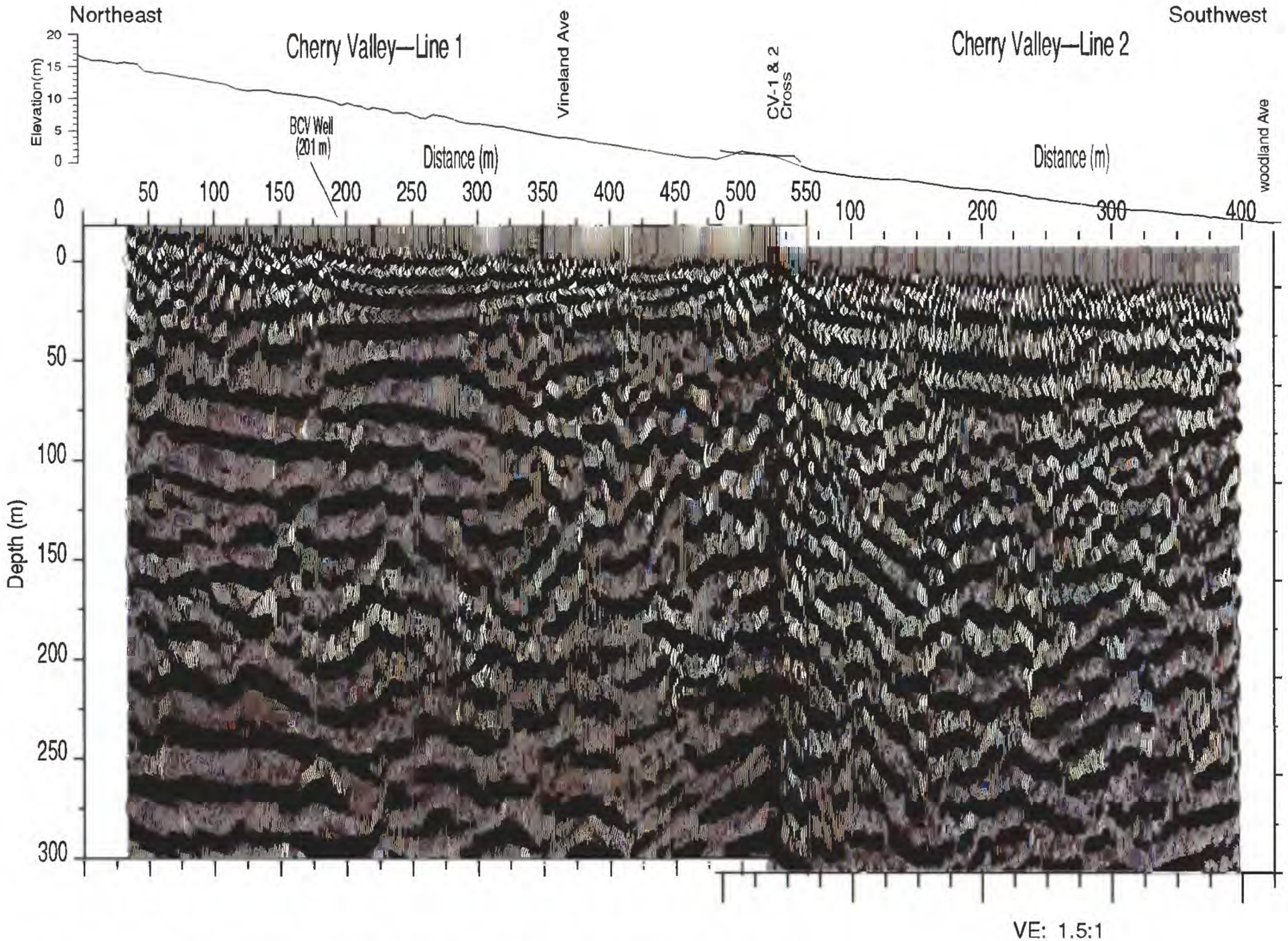

Fig. 22. Stacked and migrated seismic reflection profiles along lines 1 and 2.

Most of the apparent faults appear to extend upward into the Quaternary alluvium, suggesting that faulting is at least Quaternary in age. Given that these profiles were acquired principally within the creek bed, it is likely that the uppermost sediments are only tens to hundreds of years in age, and where the near-surface sediments are apparently vertically offset, the faulting may also be only tens to hundreds of years in age.

Although the layers appear to have been faulted and vertically offset, most can be traced laterally across the profile. In the upper 50 m, this continuity of reflectors suggests that the fine-grained layers that inhibit the downward flow of groundwater are present along the lengths of CV-1 and CV-2.

Interpreted Refraction Section

Seismic velocity models along CV-1 and CV-2 were developed by inverting first-arrival refractions using an algorithm written by Hole (1992) (Fig. 24). Approximately 36,000 seismic traces were used to derive the velocity models. Velocities range from about 400 m/s at the surface to about 1600 m/s at depths of about 75 m. The correlations between the velocity data and the borehole lithologies suggest that the Quaternary Alluvium unit ranges in velocity from about 300 m/s to 800 m/s, and the Older Alluvium unit ranges between 600 m/s to 1500 m/s. Velocity data are available only for the top of the Old Red Gravel unit, where the velocity ranges between 1500 m/s and 2000 m/s. Along CV-1 and CV-2, velocities corresponding to the Old Red Gravel occur only northeast of meter 175 of CV-1 and likely results from vertical uplift along a fault at meter 175. This apparent fault is also suggested by offset reflectors in the reflection section (Fig. 23); thus, both the reflection and refraction data independently suggest the presence of faulting and uplift in the vicinity of meter 175 of CV-1.

Combined Reflection/Refraction Section

The combined seismic velocity and reflection images are useful in understanding the subsurface because the velocity information constrains the range of subsurface materials (e.g., sediment or rock) and their physical state (such as saturated or unsaturated), and the reflection image provides structural information (Fig. 25). Both the velocity data and the reflection data show anomalies that suggest lateral changes in lithology across meter 175. Specifically, higher velocities are observed northeast of meter 175, which suggest that the top of the Old Red Gravel is structurally higher northeast of meter 175. This observation is consistent with our interpretation of a fault at meter 175 that has vertically displaced strata on either side of the fault (Fig. 23). The probable fault near meter 175 may be part of the Banning fault as mapped by Matti et al. (1992).

The 1500 m/s contour may be significant because it is the velocity expected for water-saturated, unconsolidated sediments (Schon, 1996). If the 1500 m/s contour outlines the depth to water-saturated sediments, it probably

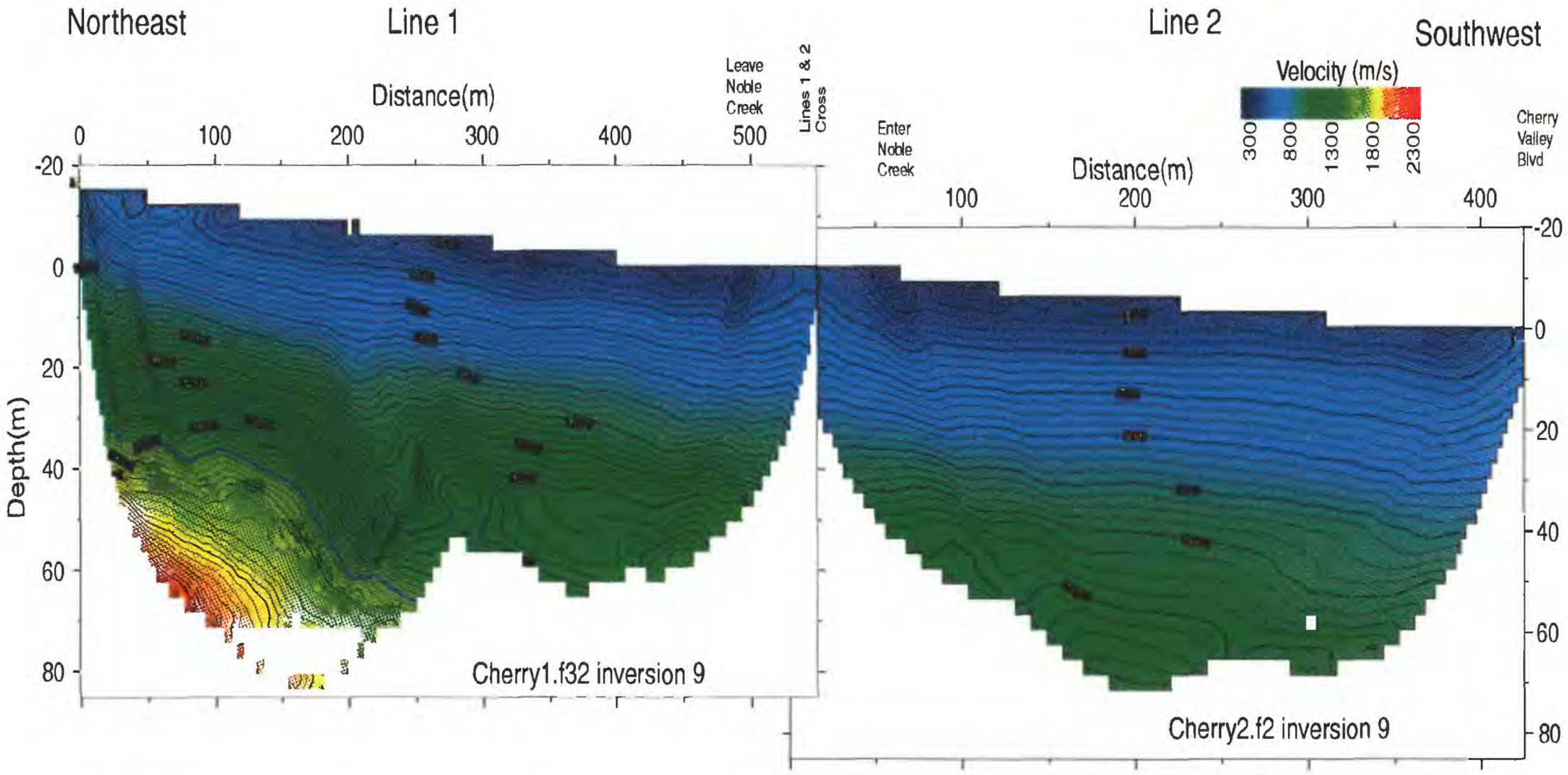

Fig. 24. Seismic velocity inversion model along Lines 1 and 2 for the upper 80 m. Velocities are in meters per second.

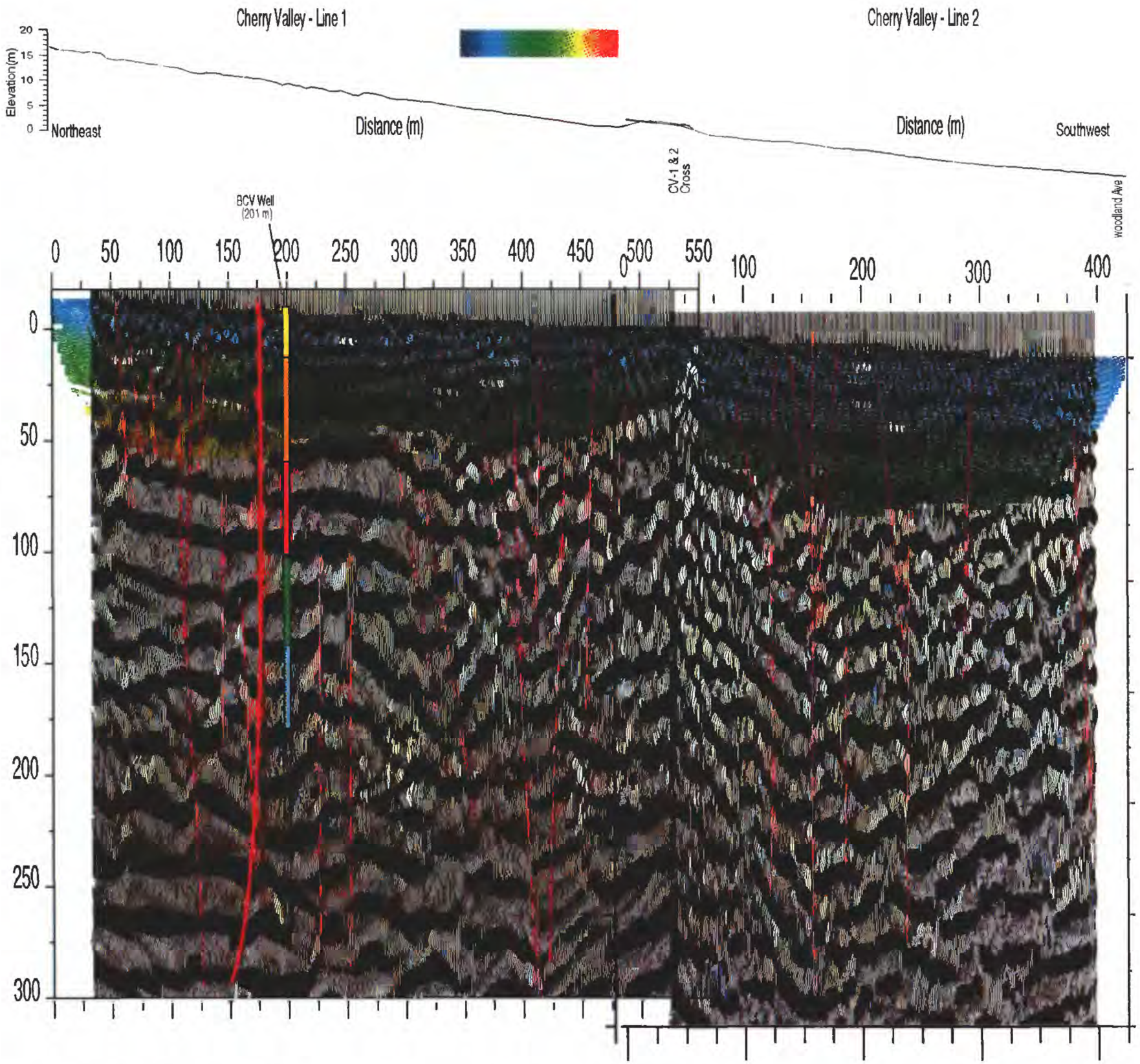

Fig. 25. Combined seismic reflection and refraction images along Lines 1 and 2. Interpreted faults are shown as red lines. Velocity contours are in m/s. The 1500 m/s contour is shown in white along line 1.

represents a perched water table because a deeper water table was found in the BCV well (Fig. 23).

Along profiles CV-1 and CV-2, the 1500 m/s contour occurs within the upper 80 m only northeast of meter 175, suggesting the possible perched water table is structurally lower to the southwest.

Profiles CV-3 and CV-4

Seismic Reflection Interpretation

Stacked, migrated, and interpreted seismic reflection images of the upper 300 m (~1000 ft) along profiles CV-3 and CV-4 are shown in figures 26 and 27 respectively. Profiles CV-3 and CV-4 were acquired separately, but they have been joined where the two profiles cross. Because CV-3 overlapped CV-4 by about 75 m, it is possible to make correlations between reflections from each line. Both seismic profiles crossed the artificial fill and concrete lining along Little San Gorgonio Creek, causing a velocity pull-up effect, whereby, reflectors appear closer to the surface. A different datum was used for CV-3 than was used for CV-4 because the datum at each line is relative to its topographically lowest geophone.

These data show reflectors that are similar to those observed along profiles CV-1 and CV-2, suggesting that the same principal lithologic units identified in CV-1 and CV-2 are present to the northwest along CV-3 and CV-4. Three wells, Test Wells 1, 2, and 3, are located in the vicinity of profiles CV-3 and CV-4. Boyle Engineering Corporation (1992) used the same category of lithologic units in the BCV and Test wells. We used their description of lithologic units and correlated them with reflectors in the seismic data where the seismic profile crossed or approached the wells. From the description of the lithologic units within the wells, we "mapped" their lateral variation along the profiles (Fig. 27).

Apparent faults are indicated by abrupt vertical offsets in a series of layers. The greatest offset appears to occur between meters 0 and 200 along CV-3, with vertical offsets of about 50 m. This series of apparent faults may be related to the apparent faults observed on the northeastern end of CV-1. The locations of the apparent faults on both seismic sections are consistent with the mapped location of the Banning Fault, as suggested by Matti et al. (1992).

Although there appear to be minor vertical offsets of layers from about meter 200 of CV-3 to the end of CV-4, the water table is not significantly offset. Most of the layers along the southwestern part of CV-3 and all of CV-4 appear to be laterally continuous. In particular, the near surface fine-grained layers that impede surface recharge of the aquifer are continuous across both profiles.

Seismic Refraction Interpretation

Seismic velocity models for CV-3 and CV-4 are shown in figure 28. More than 45,000 traces were used to derive the velocity models. Maximum velocities range from about 500 m/s near the surface to about 2000 m/s at

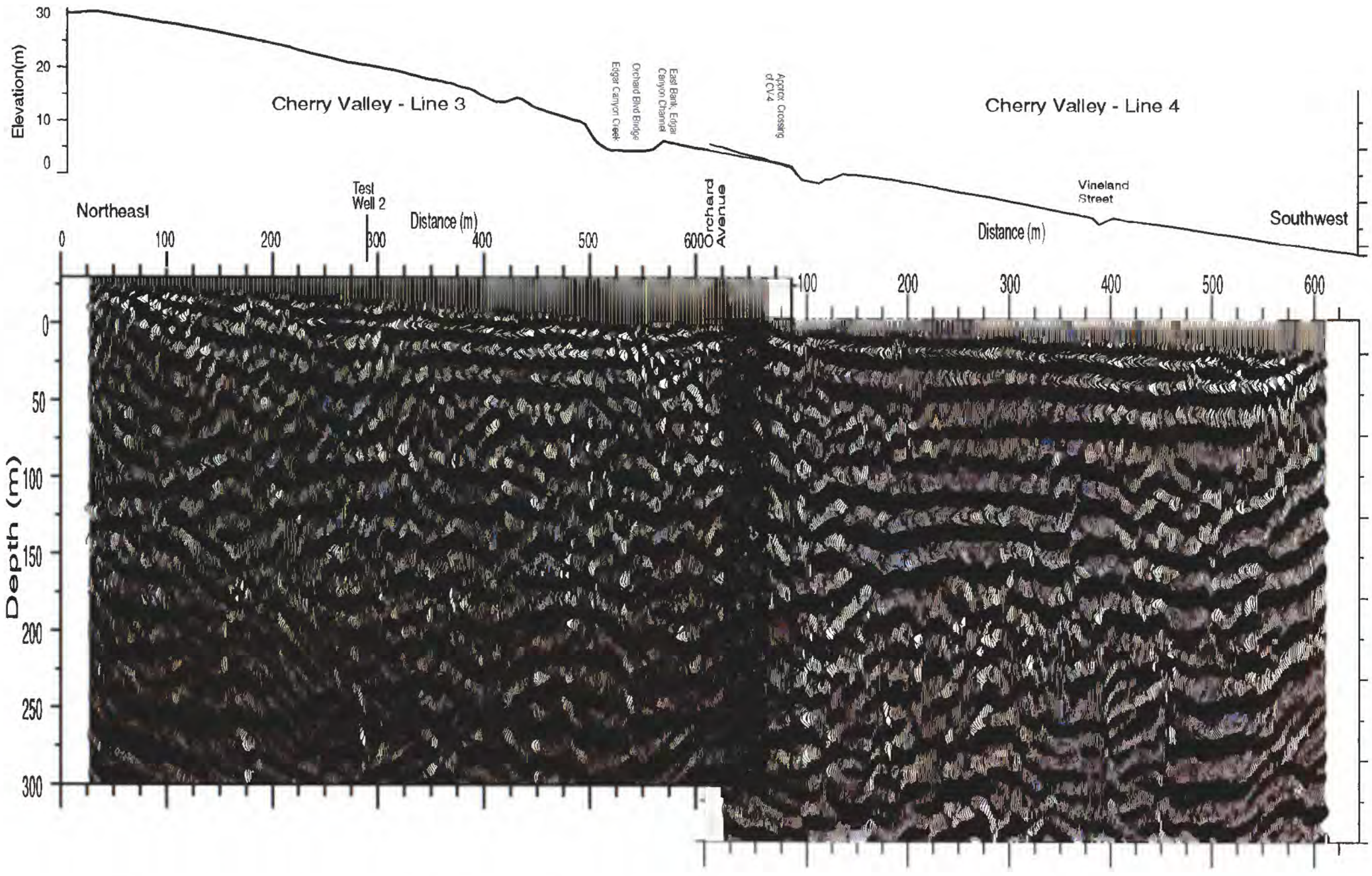

Fig. 26. Stacked and migrated seismic reflection image along Lines 3 and 4.

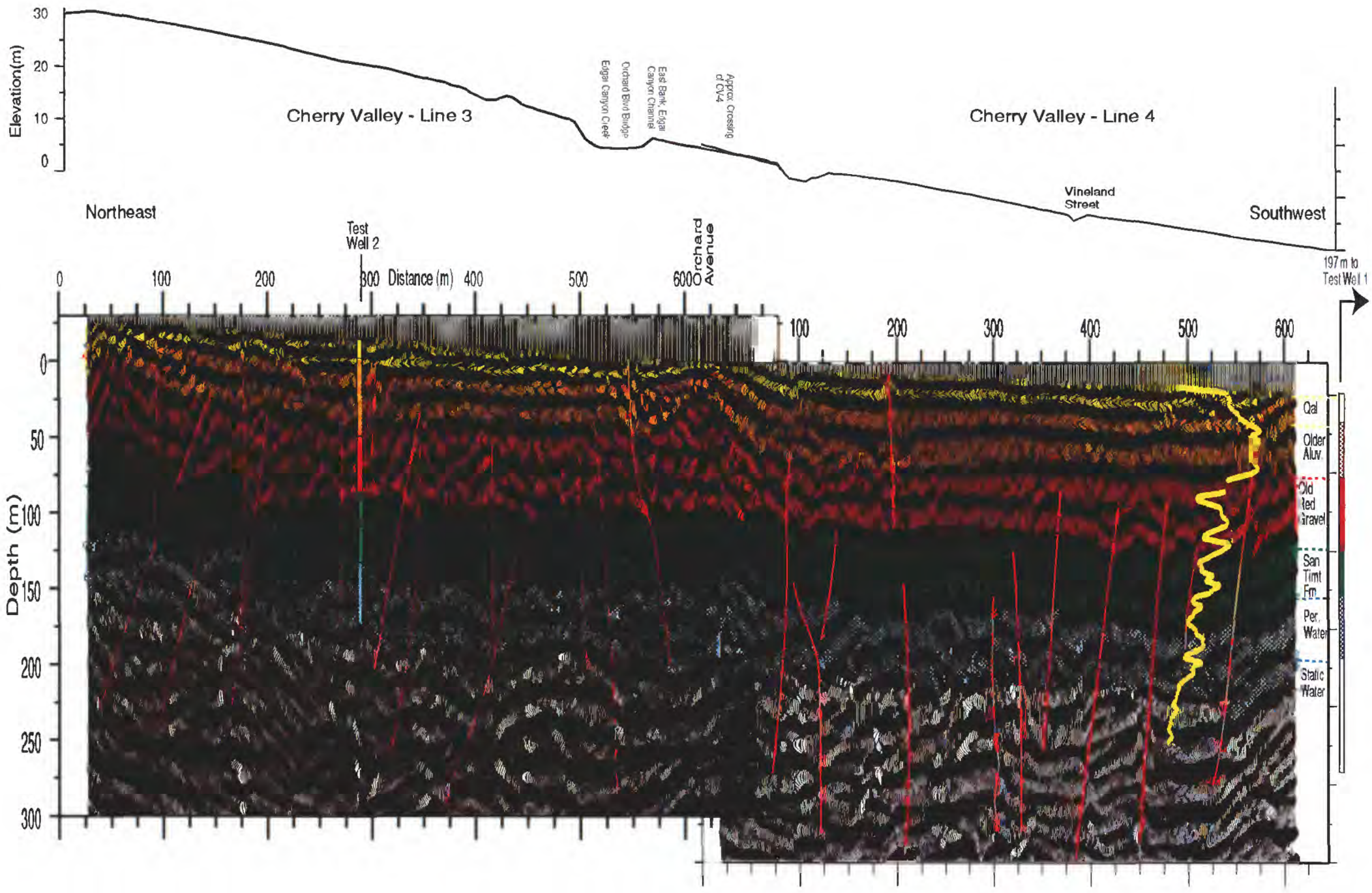

Fig. 27. Migrated and interpreted seismic reflection image along Lines 3 and 4 with the location of Test Wells 1 and 2. Colors denote stratigraphic units described in the text. Interpreted faults are shown as red lines. A resistivity log from Test Well 1 is shown in yellow.

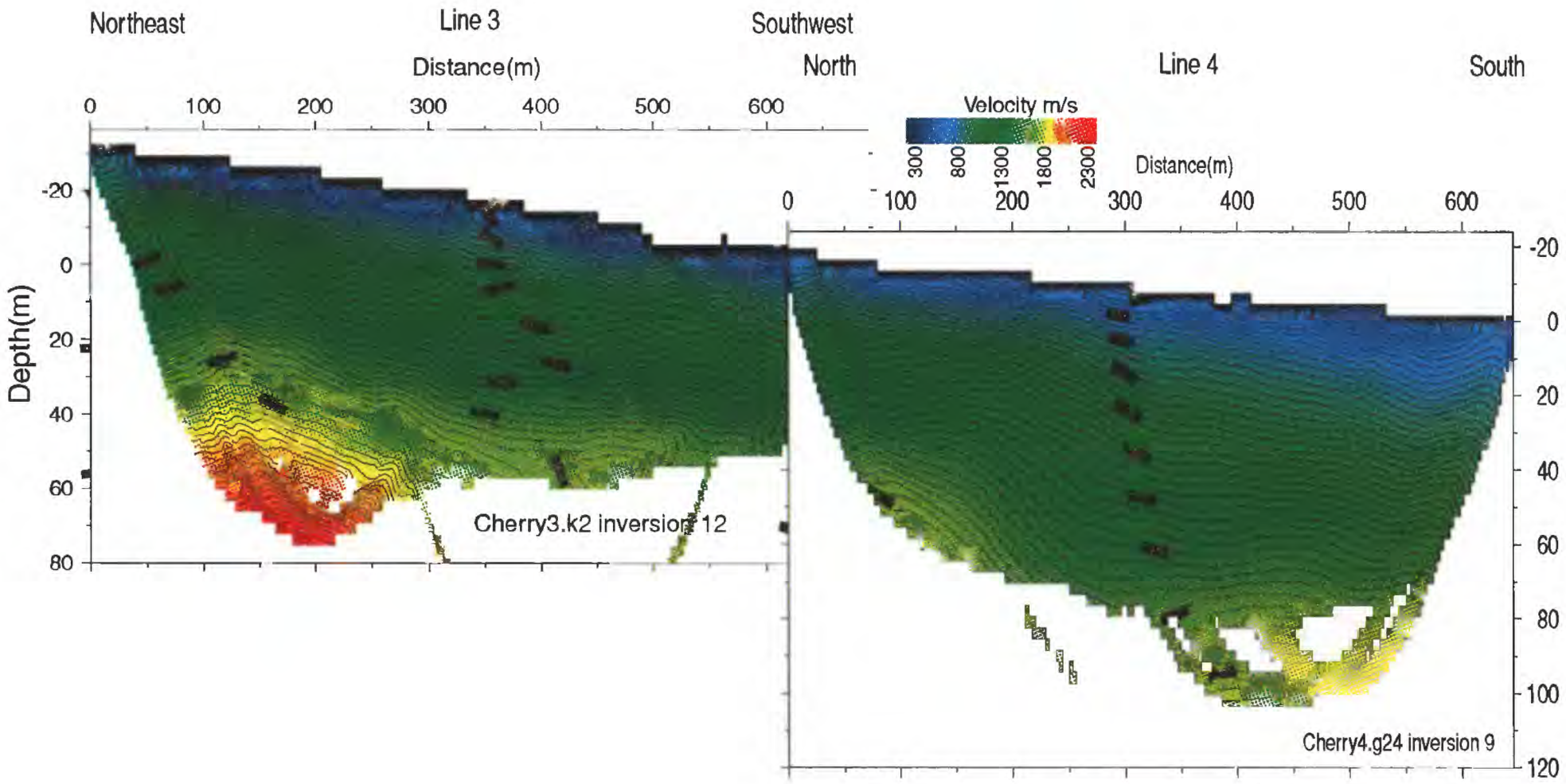

Fig. 28. Seismic velocity inversion model along Lines 3 and 4. Velocities are in meters per second.

depths of about 140 m. The relatively low velocities suggest that most of the subsurface above 140 m is composed largely of unconsolidated sediments.

Velocities ranging from about 300 m/s to about 800 m/s appear to correlate with the Quaternary Alluvium unit, and velocities ranging from about 800 to 1500 m/s correlate with the Older Alluvium unit. Velocities in excess of about 1500 m/s correspond to the Old Red Gravel. Maximum velocities of ~2000 m/s are observed only within the northeasternmost 250 m of CV-3 at depths of about 60 m (Fig. 27). Southwest of meter 250, the velocities are lower, and the velocity contours appear to be disrupted. These disrupted velocity contours may be indicative of a fault that has placed the Old Red Gravel unit (with higher velocities) higher in the section to the northwest. This interpretation is consistent with the seismic reflection data (Fig. 27). At about meter 200 along CV-4, the velocity contours dip sharply to the south, whereby, the lower-velocity (< 1500 m/s) sediments are thicker (Fig. 28). This thickening of the Quaternary and Older Alluvium units can also be seen on the seismic reflection image near meter 200 of CV-4 (Fig. 27).

Combined Reflection/Refraction Section

The seismic velocity model shown in figure 28 has been superimposed onto the seismic reflection image shown in figure 27 (Fig. 29). The combined image shows that apparent faults near meter 200 along CV-3 largely limit the southwestern extent of the ~2000 m/s velocity contour at 60 m depth. Similar apparent faults between meter 100 and 200 along CV-4 mark the southern limit of the 1500+ m/s velocity contours. These correlations suggest that the Old Red Gravel is structurally lower along two zones of faulting to the southwest. The 1500 m/s contour may correspond to a perched aquifer on top of the Old Red Gravel and can be traced along most of profiles CV-3 and CV-4 at depths ranging from about 50 m to 80 m below the ground surface. This interpretation is somewhat consistent with borehole data from Test Well 2, which shows a perched water table at about 58 m depth (bgs).

Summary and Conclusions

Using the classification by Boyle Engineering Corporation (1992), we identified a series of reflectors that correlate with the lithologic units found in the boreholes. These lithologic units appear to be laterally continuous but vertically offset by faults in numerous locations. Boreholes located near the seismic lines indicate that the upper 50 m (~165 ft) of the subsurface contain a series of fine-grained layers that do not permit efficient downward percolation of surface water. The seismic profiles along Noble Creek and Little San Gorgonio Creek suggest that these fine-grained layers are laterally extensive, extending along the entire length of all profiles. Thus, it is unlikely that relocation of the existing recharging ponds along or between profiles CV-1 through CV-4 will yield better sites for surface recharging.

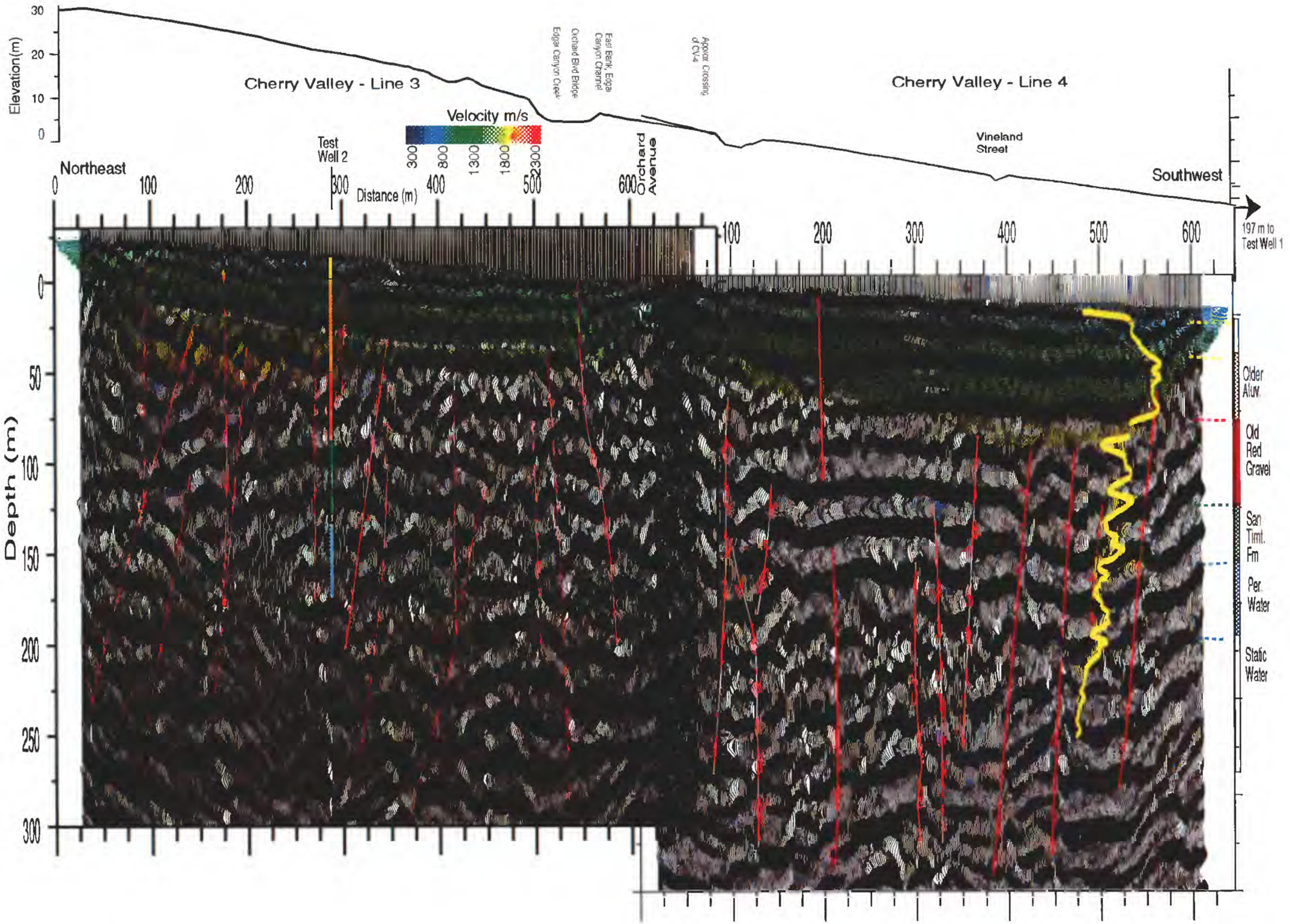

Fig. 29. Migrated seismic reflection image along Lines 3 and 4 with the velocity image superimposed. Velocities are in meters per second. The 1500 m/s contour is shown in white.

The combination of near-surface, clay-rich layers and abundant faulting may make surface recharging of the deeper aquifer difficult, as the clay-rich layers would tend to prevent downward percolation of water, and the faults would tend to segment the aquifer. Segmentation of the aquifer by faulting may inhibit recovery of recharge water from a single well, making it necessary to drill multiple recovery wells across large faults. However, in some instances, faults along the seismic line may not have sufficiently offset the deeper aquifer layers in a vertical sense, or the faults may not generate enough of an aquitard to prevent flow across the fault traces. The faults that offset the water table are likely be problematic for hydrogeologic concerns. The static water table located at about 150 m (492 feet) is vertically offset by faults at numerous locations, with individual vertical offsets of as much as 25 m and cumulative vertical offsets of as much as 50 m along a series of faults.

A perched water table was found in some wells in the area at depths of about 50 to 60 m (A. Christensen, pers comm., 1999). The seismic velocity data also show evidence (1500 m/s contour) of a perched water table in the 50- to 60-m depth range along profiles CV-3 and CV-4. However, along profiles CV-1 and CV-2, only the northeasternmost 200 m of profile CV-1 show evidence of such a perched water table in the upper 60 m. There was no clear evidence of a perched water table in the upper 60 m along the remainder of profile CV-1 or along profile CV-2. The perched water table is apparently associated with the top of the Old Red Gravel, which is higher in velocity and probably more compacted or consolidated.

The seismic profiles show appreciable evidence of faulting along both Noble and Little San Gorgonio creeks. Some of the imaged faults have vertical offsets in stratigraphy of 50 m or more, suggesting that the faults are laterally extensive. Matti et al. (1992) mapped numerous faults in the area of our profiles, and they suggest that the Banning strand of the San Andreas fault trends through the area near profiles CV-1 and CV-3. Based on the seismic images and the mapping by Matti et al. (1992), we suggest that the Banning fault is probably a zone of individual faults that extends 1 km or more in width. Although the Banning fault is covered by alluvium in the vicinity of our seismic profile, based on geologic observation, Matti et al. (1992) also suggest that the Banning fault does not consist of a single strand. Instead, they suggest that the fault zone consists of both thrust and strike-slip components. Such tectonism is likely to produce faults over a wide area, such as those observed on the seismic images. Because profiles CV-1 and CV-3 are nearly 0.5 km apart, it is difficult to correlate individual faults, but if the faults located at about meter 175 along CV-1 and between meters 100 and 200 on CV-3 are the same limited zone of faulting, then these faults may represent the principal zone of faulting along the Banning fault. Such a principal zone of faulting would trend approximately N 45° W, which is approximately the local trend of the thrust component of the Banning fault as mapped by Matti et al. (1992) in the vicinity of the seismic profiles.

For purposes of earthquake hazard assessment, the faults that extend from the surface to greater depths are of more interest. Some of the imaged

faults may pose a significant hazard to the infrastructure in Cherry Valley and should be examined more closely. The seismic images suggest that a number of the imaged faults extend to within two meters of the surface, if not entirely to the surface. Ongoing sedimentation in the creek bed and the shallow extent of these faults suggest that the faults are active. One indication that these faults are active may be the apparent westward offset in Little San Gorgonio Creek across Orchard Avenue: also, the seismic images indicate faulting there. The proximity of numerous homes, a fire station, roads, and other lifelines over the surface trace of these faults demonstrates the need to better understand the subsurface structure beneath cities throughout southern California.

Near-surface P-wave velocities are as low as 300 m/s, and corresponding S-wave velocities are likely to be much lower. These low velocities indicate that the sediments are unconsolidated, and because they are several hundred meters thick, the low-velocity sediments will likely amplify seismic waves. Such amplified seismic waves could result in strong shaking from blind faults beneath the Cherry Valley area or from large-magnitude earthquakes on other faults of the San Andreas fault system. Several lifelines including the California River aqueduct, gas lines, power lines, and an interstate highway trend through San Gorgonio Pass in the vicinity of Cherry Valley. Strong shaking from large-magnitude earthquakes on the San Andreas fault or smaller-magnitude earthquakes on blind faults beneath Cherry Valley could potentially disrupt these lifelines, thereby impacting the larger urban centers of southern California.

Data Availability

The data are available as shot gathers with elevation and timing corrections applied in SEG-Y format from R.D. Catchings at the address in the front of this report.

Acknowledgments

This study was a cooperative effort between the US Geological Survey (Geologic and Water Resources Divisions) and the SGPWA. We thank Tom Burdette, Jeff Dingler, Katherine Favret, Jamie Fenimore, Joseph Grow, Monique Jaasma, Gernot Laganda, Nicole Lautze, Janice Murphy, Keith Rice, Jose Rodriguez, and Marjan Rotting for assistance in acquiring the seismic data. The project was funded by the San Gorgonio Water District, and we particularly thank Steve Stockton for his foresight and assistance.

References

Borcherdt, R. D., and G. Glassmoyer, 1994, Influences of local geology on strong and weak ground motions recorded in the San Francisco Bay region and their implications for site-specific building code provisions, in the Loma Prieta, California Earthquake of October 17, 1989 - Strong Ground Motion, US Geol. Surv. Profess. Pap. 15512-A, 77-109.

Catchings, R. D., 1998, High-resolution seismic imaging for environmental and earthquake hazards assessment at the Raychem Site, Menlo Park, California, U. S. Geol. Surv. Open-File Report 98-146, 37 pp.

Catchings, R. D., M. R. Goldman, W. H. K. Lee, M. J. Rymer and D. J. Ponti, 1998, Faulting Apparently Related to the 1994 Northridge, California, Earthquake and Possible Co-Seismic Origin of Surface Cracks in Potrero Canyon, Los Angeles County, California, Seis. Soc. America Bull., v. 88, p. 1379-1391.

Hauksson, E., L. M. Jones, and K. Hutton, 1995, The 1994 Northridge earthquake sequence in California: Seismological and tectonic aspects, J. Geophys. Res., 97, 12,335-12,355.

Hole, J.A, 1992, Nonlinear high-resolution three-dimensional seismic travel time tomography, J. Geophys. Res., v. 97, p. 6553-6562.

Jennings, C.W., R.G. Strand, and T.H. Rogers, 1977, Geologic Map of California: California Geologic Data Map Series, Map # 2, map scale 1:750,000.

Magistrale, H., and C. Sanders, 1996, Evidence from precise earthquake hypocenters for segmentation of the San Andreas fault in San Gorgonio Pass, J. Geophys. Res., v. 101, p. 3031-3044.

Matti, J. C., D. M. Morton, and B. F. Cox, 1992, The San Andreas fault system in the vicinity of the central Transverse Ranges province, southern California, U. S. Geological Survey Open-file Report 92-354, 49 pp.

Schon, J.H., 1996, Physical properties of rocks: Fundamentals and principles of petrophysics, Handbook of Geophysical Exploration (Seismic Exploration), v.18, Pergamon Press, Elsevier Science, Inc., Tarrytown, New York, 583 pp.

Appendix A

Global Positioning System (GPS) points for seismic lines

LINE 1

Station 1 (shot point 1)
N 33 58' 14.05"
W 116 58' 13.39"
Elev 2861

Station 28 (geophone 1)
N 33 58' 15.96"
W 116 58' 12.29"
Elev 2822

Station 86 (road)
N 33 58' 20.29"
W 116 58" 09.98"
Elev 2881

Station 205 (geophone 178)
N 33 58" 30.69"
W 116 58" 05.24"
Elev 2922

Station 221 (shotpoint 111)
N 33 58" 31.33"
W 116 58' 04.68"
Elev 2922

Station 229 (shotpoint 115, not used)
N 33 58' 31.33"
W 116 58' 04.24"
Elev 2918

LINE 2

Station 1 (sp 1)
N 33 58' 17.93"
W 116 58' 10.26"
Elev 2868

Station 171 (sp 86) (~5 ft N of Road)
N 33 58' 07.79"
W 116 58' 21.49"
Elev 2826

LINE 3

Station 1 (sp 1)
first shot point
N 33 58' 49.60"
W 116 58' 15.33"
Elev 2976

Station 213 (sp 107)
directly under bridge
N 33 58' 33.55"
W 116 58' 22.85"
Elev 2933

Station 277 (sp 139)
last shotpoint
N 33 58' 28.70"
W 116 58' 25.06"
Elev 2877

LINE 4

Station 1 (first shot point)
N 33 58' 33.21"
W 116 58' 24.76"
Elev 2880

Station 8 (middle of road)
N 33 58' 32.58"
W 116 58' 24.87"
Elev 2862

Station 45 (crossover line 3)
N 33 58' 29.00"
W 116 58' 24.78"
Elev 2857

Station 131 (middle of road)
N 33 58' 20.63"
W 116 58' 24.92"
Elev 2841

Station 215 (last shot point)
N 33 58' 12.45"
W 116 58' 24.95"
Elev 2824

Appendix B

Locations and elevations for seismic lines. Distances and elevations are relative to first shot point.

Cherry Valley Line 1

Shot No.	Station No.	Shot Dist. (m)	Shot Elev. (m)		Station No.	Receiver Dist. (m)	Receiver Elev. (m)
1001	1	0	0		28	67.25	0.69
1002	3	4.88	0.94		29	69.82	0.73
1003	5	9.48	0.99		30	72.19	0.82
1004	7	14.66	0.93		31	74.68	0.98
1005	9	19.78	1.04		32	77.17	1.03
1006	11	24.75	1.15		33	79.47	0.89
1007	13	29.76	1.27		34	82.22	0.88
1008	15	34.85	1.37		35	84.84	0.9
1009	17	39.67	1.49		36	87.21	0.9
1010	19	44.47	1.68		37	89.46	0.96
1011	27	64.56	0.41		38	92.25	1.28
1012	29	69.41	0.63		39	94.61	1.15
1013	31	74.59	0.69		40	97.29	1.2
1014	33	79.65	0.71		41	99.71	1.26
1015	35	84.61	0.75		42	102.28	1.31
1016	37	89.41	0.84		43	104.89	1.37
1017	39	94.88	1.1		44	107.15	1.52
1018	45	109.58	1.61		45	109.7	1.74
1019	47	114.47	1.85		46	112.2	1.76
1020	49	119.53	1.96		47	114.82	1.8
1021	51	124.49	2.12		48	117.32	1.86
1022	53	129.41	2.3		49	119.79	1.95
1023	55	134.39	2.44		50	122.26	2.03
1024	57	139.45	2.65		51	124.77	2.1
1025	59	144.44	2.8		52	127.3	2.17
1026	63	154.48	3.07		53	129.79	2.29
1027	65	159.55	3.2		54	132.3	2.33
1028	67	164.2	3.49		55	134.71	2.4
1029	69	169.43	3.71		56	137.24	2.5
1030	71	174.45	3.76		57	139.72	2.63
1031	73	179.4	3.92		58	142.27	2.71
1032	75	184.41	3.94		59	144.72	2.8
1033	77	189.27	4.13		60	147.24	2.84
1034	79	194.26	4.3		61	149.75	3.01
1035	81	199.26	4.5		62	152.2	3.1
1036	83	204.25	4.7		63	154.74	3.14
1037	89	219.24	5.26		64	157.21	3.21
1038	91	224.58	5.56		65	159.68	3.35
1039	93	229.45	5.57		66	161.97	3.52
1040	97	239.36	5.93		67	164.68	3.51
1041	99	244.4	6.02		68	167.13	3.75
1042	101	249.53	6.04		69	169.38	3.6
1043	103	254.41	6.16		70	172.11	3.84
1044	105	259.32	6.36		71	174.62	3.71
1045	107	264.46	6.82		72	177.15	3.94
1046	109	269.3	7.12		73	179.65	4.01
1047	111	274.37	7.3		74	182.12	4.02
1048	113	279.25	7.43		75	184.42	4.16
1049	115	284.48	6.84		76	187.11	4.21
1050	117	289.14	6.98		77	189.62	4.29
1051	119	294.35	7.36		78	192.06	4.32
1052	121	299.23	7.78		79	194.61	4.4
1053	125	309.53	7.69		80	197.1	4.45
1054	127	314.41	8.19		81	199.6	4.5
1055	129	319.25	8.34		82	202.1	4.6
1056	131	324.43	8.56		83	204.6	4.7
1057	133	329.18	8.25		84	207.1	4.75
1058	135	334.43	8.78		85	209.6	4.8
1059	137	339.07	8.88		86	212.1	4.85
1060	139	344.24	9.27		87	214.5	4.9
1061	141	349.15	8.91		88	216.99	5.02

1062	143	354.02	9.42
1063	145	359.29	9.72
1064	147	364.57	10.01
1065	149	369.54	10.25
1066	151	374.1	10.27
1067	153	379.33	10.43
1068	155	384.27	10.6
1069	157	389.23	10.68
1070	159	394.16	10.8
1071	161	399.41	10.91
1072	163	404.23	11.26
1073	165	409.06	11.34
1074	167	413.97	11.28
1075	169	418.99	11.17
1076	171	424.24	11.32
1077	173	429.15	11.5
1078	175	434.34	12.02
1079	177	439.04	12.34
1080	179	444.03	12.43
1081	181	449.13	12.6
1082	183	453.81	12.87
1083	185	458.9	13.04
1084	187	463.94	13.14
1085	189	468.97	13.38
1086	191	473.68	13.52
1087	193	478.89	13.75
1088	195	483.99	13.94
1089	197	489.06	13.93
1090	199	493.8	14.12
1091	201	498.82	14.28
1092	203	503.91	15.37
1093	205	508.97	15.47
1094	207	513.89	15.63
1095	209	519.02	15.48
1096	211	523.83	15.63
1097	213	528.92	15.86
1098	215	533.56	15.93
1099	217	538.74	15.96
1100	219	543.76	16.28
1101	221	548.89	16.75

89	219.49	5.14
90	221.98	5.23
91	224.55	5.4
92	226.95	5.68
93	229.5	5.6
94	232.01	5.6
95	234.47	5.82
96	237.09	5.9
97	239.53	5.99
98	242.04	5.98
99	244.64	6.04
100	246.97	6.02
101	249.5	6.03
102	251.91	6.06
103	254.43	6.22
104	257.11	6.27
105	259.47	6.37
106	261.85	6.71
107	264.34	6.83
108	266.89	6.87
109	269.26	6.99
110	271.9	7.19
111	274.28	7.2
112	276.81	7.23
113	279.27	7.12
114	281.97	6.76
115	284.51	6.85
116	286.97	6.9
117	289.22	7
118	291.92	7.52
119	294.21	7.66
120	296.77	7.73
121	299.36	7.81
122	301.99	7.72
123	304.46	7.63
124	306.9	7.69
125	309.41	8.05
126	311.96	8.24
127	314.38	8.24
128	316.74	8.31
129	319.3	8.2
130	321.93	8.25
131	324.29	8.56
132	326.96	8.68
133	329.43	8.7
134	332.07	8.61
135	334.46	8.88
136	336.73	8.89
137	339.23	8.77
138	341.77	9.1
139	344.39	9.24
140	347.01	9.32
141	349.17	9
142	352.02	9.1
143	354.23	9.4
144	356.86	9.69
145	359.16	9.85
146	361.76	9.84
147	364.29	9.93
148	366.74	9.98
149	369.21	10.07
150	371.85	10.22
151	374.35	10.27
152	376.75	10.34
153	379.33	10.5
154	381.62	10.54
155	384.21	10.71
156	386.64	10.67

157	389.22	10.72
158	391.59	10.76
159	394.21	10.9
160	396.73	10.99
161	399.22	11.1
162	401.78	11.21
163	404.18	11.35
164	406.54	11.31
165	408.92	11.45
166	411.66	11.02
167	413.9	11.09
168	416.57	11.15
169	419.24	11.19
170	420.8	11.24
171	424.2	11.32
172	426.35	11.82
173	428.8	11.92
174	431.39	12.07
175	434.05	11.92
176	436.42	12.43
177	438.95	12.51
178	441.48	12.5
179	443.97	12.54
180	446.53	12.62
181	449.09	12.79
182	451.56	12.76
183	453.9	12.9
184	456.18	13.21
185	458.84	13.45
186	461.3	13.13
187	463.82	13.2
188	466.41	13.22
189	468.93	13.38
190	471.42	13.48
191	473.87	13.53
192	476.12	13.58
193	478.83	13.66
194	481.11	13.73
195	483.76	13.93
196	486.33	14.09
197	489.08	14.21
198	491.3	14.27
199	493.71	14.28
200	496.19	14.47
201	498.62	14.48
202	501.42	15.32
203	503.83	15.4
204	506.32	15.51
205	509	15.64

Appendix C

Cherry Valley Line 2

Shot No.	Station No.	Shot Dist. (m)	Shot Elev. (m)	Station No.	Receiver Dist. (m)	Receiver Elev. (m)
1001	1	0	14.55	30	72.7	10.5
1002	3	5.04	14.32	31	75.24	10.51
1003	5	10.38	14.14	32	77.7	10.52
1004	7	15.32	14.01	33	80.15	10.42
1005	9	20.31	14.04	34	82.52	10.25
1006	11	25.41	13.93	35	85.12	10.22
1007	13	30.22	13.9	36	87.77	10.03
1008	15	35.59	13.69	37	90.24	9.94
1009	17	40.32	13.52	38	92.61	9.83
1010	19	45.44	13.15	39	95.06	9.79
1011	29	70.02	10.75	40	97.54	9.7
1012	31	74.78	10.46	41	99.92	9.58
1013	33	80.26	10.41	42	102.73	9.4
1014	35	85.31	10.1	43	105.15	9.34
1015	37	90.04	9.93	44	107.51	9.26
1016	39	95.31	9.76	45	110.05	9.22
1017	41	99.96	9.5	46	112.67	9.16
1018	43	105.26	9.36	47	115.05	9.01
1019	45	110.07	9.3	48	117.59	9.04
1020	47	115.26	9.11	49	119.98	8.95
1021	49	120.07	9	50	122.43	8.87
1022	51	124.97	8.92	51	124.92	8.82
1023	53	130.23	8.84	52	127.48	8.77
1024	55	135.29	8.9	53	129.82	8.52
1025	57	140.2	8.85	54	132.42	8.61
1026	59	145.29	8.53	55	135.09	8.6
1027	61	150.04	8.47	56	137.73	8.55
1028	63	155.17	8.25	57	139.86	8.57
1029	65	160.16	8.05	58	142.32	8.66
1030	67	165.19	7.88	59	144.86	8.56
1031	69	170.15	7.63	60	147.22	8.45
1032	71	175	7.39	61	149.88	8.4
1033	73	180	7.21	62	152.51	8.35
1034	75	184.99	7.13	63	154.98	8.2
1035	77	189.79	7.16	64	157.59	8.16
1036	79	194.83	6.94	65	160.03	7.81
1037	81	199.88	6.77	66	162.56	7.82
1038	83	205.01	6.76	67	165.1	7.7
1039	85	209.68	6.54	68	167.75	7.42
1040	87	214.83	6.4	69	169.98	7.36
1041	89	219.7	6.15	70	172.27	7.31
1042	91	224.96	6.05	71	174.86	7.22
1043	93	229.74	5.72	72	177.42	7.16
1044	95	234.74	5.62	73	180	7.1
1045	97	239.59	5.26	74	182.56	7.06
1046	99	244.81	5.09	75	184.91	7.03
1047	101	249.77	5.03	76	187.14	6.98
1048	103	254.71	4.73	77	189.69	6.98
1049	105	259.77	4.58	78	192.33	6.92
1050	107	264.76	4.45	79	194.89	6.79
1051	109	269.66	4.24	80	197.44	6.57
1052	111	274.79	4.12	81	200.06	6.57
1053	113	279.86	3.98	82	202.25	6.53
1054	115	284.87	3.7	83	204.92	6.58
1055	117	289.84	3.63	84	207.48	6.42
1056	119	294.85	3.52	85	209.71	6.37

1057	123	304.8	3.2
1058	125	309.74	3.09
1059	127	314.82	2.89
1060	129	319.74	2.85
1061	133	329.82	2.78
1062	135	334.89	2.6
1063	137	340.15	2.48
1064	139	344.93	2.28
1065	141	349.8	2.11
1066	143	354.58	1.97
1067	145	359.85	1.98
1068	147	364.83	1.82
1069	149	369.62	1.75
1070	151	374.87	1.41
1071	153	379.7	1.49
1072	155	384.71	1.24
1073	157	389.7	1.17
1074	159	394.66	0.99
1075	161	399.79	1.01
1076	163	404.44	0.84
1077	165	409.73	0.72
1078	167	414.64	0.45
1079	169	419.83	0.45
1080	171	424.76	0.3

86	212.27	6.24
87	214.91	6.14
88	217.37	6.08
89	219.76	6.09
90	222.36	5.75
91	224.82	5.69
92	227.44	5.67
93	229.91	5.6
94	232.37	5.49
95	234.75	5.47
96	237.33	5.15
97	239.69	5.08
98	242.1	5.02
99	244.62	5
100	247.16	4.97
101	249.7	4.91
102	252.02	4.67
103	254.69	4.66
104	257.13	4.59
105	259.58	4.55
106	262.08	4.5
107	264.67	4.42
108	267.08	4.23
109	269.59	4.19
110	271.98	4.13
111	274.69	4.08
112	277.2	4.04
113	279.71	3.99
114	282	3.82
115	284.52	3.78
116	287.1	3.7
117	289.79	3.66
118	292.3	3.64
119	294.84	3.58
120	297.43	3.34
121	299.59	3.35
122	302.07	3.31
123	304.74	3.27
124	307.41	3.17
125	309.88	3.17
126	312.34	3.1
127	314.8	3.07
128	316.98	3.05
129	319.63	3
130	322.19	2.97
131	324.66	2.85
132	327.14	2.7
133	329.66	2.72
134	332.16	2.62
135	334.65	2.53
136	337.1	2.39
137	339.91	2.38
138	342.45	2.31
139	345.24	2.19
140	347.76	2.13
141	350.15	2.08
142	352.53	1.93
143	354.78	1.87
144	357.38	1.84
145	359.9	1.81
146	362.31	1.74

147	364.83	1.71
148	367.39	1.48
149	369.83	1.38

Appendix D

Cherry Valley Line 3

Shot No.	Station No.	Shot Dist. (m)	Shot Elev. (m)	Station No.	Receiver Dist. (m)	Receiver Elev. (m)
1001	1	0	30.04	23	55.42	29.64
1002	3	4.95	30.09	24	57.91	29.5
1003	5	9.94	30.17	25	60.42	29.43
1004	7	15.05	30.28	26	62.9	29.35
1005	9	20.02	30.36	27	65.33	29.25
1006	11	24.89	30.45	28	67.94	29.19
1007	13	29.98	30.38	29	70.46	29.13
1008	15	34.75	30.22	30	72.92	29.04
1009	17	39.89	30.06	31	75.6	28.95
1010	19	44.79	29.83	32	77.91	28.84
1011	21	49.92	29.67	33	80.42	28.71
1012	23	54.86	29.58	34	82.89	28.66
1013	25	59.69	29.41	35	85.45	28.57
1014	27	64.82	29.22	36	87.91	28.48
1015	29	69.82	29	37	90.44	28.42
1016	31	74.88	28.84	38	92.91	28.34
1017	33	79.84	28.69	39	95.45	28.29
1018	35	84.83	28.51	40	97.92	28.19
1019	37	89.95	28.32	41	100.37	28.15
1020	39	94.93	28.26	42	102.92	28.04
1021	41	100.03	28.1	43	105.43	27.97
1022	43	104.66	27.93	44	107.89	27.86
1023	45	109.76	27.74	45	110.41	27.8
1024	47	114.86	27.57	46	112.85	27.71
1025	49	119.79	27.4	47	115.38	27.6
1026	51	124.8	27.18	48	117.88	27.48
1027	53	129.73	26.97	49	120.42	27.39
1028	55	134.81	26.79	50	122.88	27.3
1029	57	139.86	26.61	51	125.36	27.2
1030	59	144.83	26.41	52	127.99	27.08
1031	61	149.6	26.22	53	130.44	26.96
1032	63	154.69	26	54	132.87	26.84
1033	65	159.78	25.77	55	135.36	26.76
1034	67	164.78	25.6	56	137.85	26.68
1035	69	169.78	25.35	57	140.38	26.6
1036	71	174.69	25.27	58	142.86	26.49
1037	73	179.69	25.03	59	145.4	26.41
1038	75	184.81	24.8	60	147.84	26.28
1039	77	189.84	24.63	61	150.38	26.18
1040	79	194.86	24.39	62	152.85	26.06
1041	81	199.62	24.24	63	155.36	25.96
1042	83	204.73	24.01	64	157.87	25.87
1043	85	209.95	23.74	65	160.37	25.78
1044	87	214.79	23.43	66	162.86	25.68
1045	89	219.79	23.15	67	165.35	25.59
1046	91	224.89	22.89	68	167.86	25.48
1047	93	229.72	22.62	69	170.33	25.4
1048	95	234.79	22.4	70	172.85	25.31
1049	97	239.83	22.15	71	175.37	25.23
1050	99	244.73	21.94	72	177.86	25.14
1051	101	249.82	21.69	73	180.35	25.03
1052	103	254.78	21.41	74	182.85	24.92
1053	105	259.63	21.16	75	185.32	24.82
1054	107	264.72	20.91	76	187.74	24.72
1055	109	269.64	20.79	77	190.27	24.64
1056	111	274.66	20.62	78	192.81	24.53

1057	113	279.6	20.43	79	195.33	24.43
1058	115	284.58	20.35	80	197.79	24.31
1059	117	289.63	20.14	81	200.32	24.24
1060	119	294.67	19.98	82	202.78	24.12
1061	121	299.62	19.73	83	205.3	24.01
1062	123	304.65	19.58	84	207.8	23.87
1063	125	309.67	19.38	85	210.25	23.75
1064	129	319.72	18.91	86	212.72	23.62
1065	131	324.61	18.61	87	215.27	23.47
1066	133	329.72	18.35	88	217.75	23.32
1067	135	334.59	18.1	89	220.22	23.18
1068	137	339.67	17.82	90	222.7	23.03
1069	139	344.59	17.65	91	225.16	22.9
1070	141	349.59	17.5	92	227.69	22.78
1071	143	354.64	17.28	93	230.2	22.66
1072	145	359.6	17.03	94	232.66	22.53
1073	147	364.65	16.93	95	235.17	22.42
1074	149	369.7	16.42	96	237.64	22.28
1075	151	374.7	16.18	97	240.13	22.16
1076	153	379.58	16	98	242.62	22.07
1077	155	384.49	15.62	99	245.18	21.93
1078	157	389.59	14.9	100	247.62	21.81
1079	159	394.69	14.45	101	250.08	21.68
1080	161	399.7	13.94	102	252.62	21.51
1081	163	404.58	13.56	103	255.12	21.37
1082	165	409.66	13.51	104	257.67	21.22
1083	167	414.68	13.52	105	260.24	21.05
1084	169	419.57	13.93	106	262.44	20.99
1085	171	424.58	14.3	107	265.09	20.94
1086	173	429.54	13.98	108	267.55	20.82
1087	175	434.51	13.36	109	270.04	20.76
1088	177	439.3	12.71	110	272.52	20.69
1089	179	444.25	12.27	111	275.08	20.62
1090	181	449.39	12.01	112	277.52	20.52
1091	183	454.39	11.59	113	280.05	20.4
1092	185	459.41	11.3	114	282.76	20.3
1093	187	464.29	11.02	115	285.27	20.26
1094	189	469.35	10.72	116	287.79	20.2
1095	191	474.36	10.38	117	290.31	20.15
1096	193	479.31	10.06	118	292.79	20.05
1097	195	484.27	9.9	119	295.28	19.98
1098	197	489.21	9.34	120	297.75	19.87
1099	199	494.12	7.7	121	300.24	19.76
1100	201	499.04	6.16	122	302.75	19.68
1101	203	503.91	5.37	123	305.28	19.6
1102	205	508.71	4.75	124	307.76	19.51
1103	207	513.58	4.44	125	310.25	19.42
1104	217	538.71	4.25	126	312.75	19.31
1105	219	543.65	4.29	127	315.17	19.19
1106	221	548.54	4.38	128	317.63	19.04
1107	223	553.62	4.57	129	320.2	18.88
1108	227	563.58	6.18	130	322.81	18.71
1109	229	568.82	5.86	131	325.12	18.55
1110	231	573.66	5.75	132	327.6	18.44
1111	233	578.62	5.47	133	330.13	18.32
1112	235	583.79	5.3	134	332.66	18.21
1113	237	588.64	5.04	135	335.12	18.11
1114	239	593.85	4.81	136	337.6	17.94
1115	241	598.81	4.7	137	340.12	17.83
1116	243	603.7	4.57	138	342.66	17.75
1117	245	608.59	4.42	139	345.17	17.7

1118	247	613.6	4.26
1119	249	618.48	4.01
1120	251	623.63	3.9
1121	253	628.6	3.65
1122	255	633.5	3.53
1123	257	638.61	3.3
1124	259	643.64	3.12
1125	261	648.53	2.99
1126	263	653.59	2.78
1127	265	658.55	2.62
1128	267	663.51	2.39
1129	269	668.5	2.16
1130	271	673.44	1.93
1131	273	678.47	1.57
1132	275	683.51	1.42
1133	277	688.53	0

140	347.65	17.56
141	350.06	17.46
142	352.56	17.31
143	355.1	17.19
144	357.61	17.01
145	360.05	16.98
146	362.51	16.96
147	365.01	16.93
148	367.57	16.73
149	370.06	16.43
150	372.28	16.04
151	375.22	15.97
152	377.4	15.91
153	380.03	15.7
154	382.31	15.69
155	384.8	15.03
156	387.11	14.64
157	389.9	14.72
158	392.29	14.34
159	394.87	13.91
160	397.39	13.57
161	399.85	13.56
162	402.45	13.35
163	404.92	13.27
164	407.41	13.2
165	410	13.24
166	412.44	13.23
167	415.03	13.32
168	417.59	13.3
169	419.98	13.75
170	422.35	14.32
171	424.97	14.34
172	427.43	14.22
173	429.88	14.06
174	432.32	13.78
175	434.77	13.38
176	437.23	12.99
177	439.85	12.84
178	442.28	12.33
179	444.77	12.12
180	447.24	11.99
181	449.76	11.84
182	452.24	11.71
183	454.79	11.59
184	457.53	11.55
185	459.75	11.33
186	462.26	11.16
187	464.73	10.99
188	467.2	10.83
189	469.7	10.67
190	472.21	10.54
191	474.69	10.38
192	477.17	10.24
193	479.64	10.05
194	482.17	9.9
195	484.63	9.8
196	487.02	9.74
197	489.61	9.72
198	492.07	9.11
199	494.23	8.22
200	496.56	7.18

201	498.83	6.23
202	501.24	6.03
203	504.08	5.55
204	506.61	5.21
205	509.04	4.68
206	511.45	4.6
207	513.94	4.5
208	516.38	4.38
209	518.97	4.32
210	521.46	4.19
211	524.11	4.15
212	526.51	3.92
213	528.98	3.85
214	531.51	3.79
215	534.06	3.72
216	536.49	3.71
217	538.92	3.64
218	541.43	3.64
219	544	3.95
220	546.48	4.03
221	548.95	4.14
222	551.01	4.25
223	553.59	4.38
224	555.92	4.25
225	558.41	4.44
226	560.68	5.1
227	563.6	5.36
228	566.11	5.65
229	568.65	5.68
230	571.12	5.7
231	573.54	5.6
232	576.06	5.52
233	578.64	5.38
234	581.12	5.31
235	583.63	5.2
236	586.12	5.12
237	588.63	5.1
238	591.12	4.95
239	593.63	4.81
240	596.13	4.7
241	598.63	4.65
242	601.1	4.55
243	603.6	4.48
244	606.07	4.41
245	608.65	4.38
246	611.12	4.29
247	613.63	4.21
248	616.05	4.13
249	618.6	4.02
250	621.09	3.94
251	623.63	3.83
252	626.09	3.75
253	628.6	3.67
254	631.08	3.56
255	633.57	3.45
256	636.11	3.35
257	638.58	3.27
258	641.09	3.18
259	643.61	3.08
260	646.11	3

Appendix E

Cherry Valley Line 4

Shot No.	Station No.	Shot Dist. (m)	Shot Elev. (m)	Station No.	Receiver Dist. (m)	Receiver Elev. (m)
1001	1	0	19.49	14	38.38	17.55
1002	3	6.09	19.1	15	41.39	17.41
1003	5	12.15	18.92	16	44.37	17.28
1004	11	30.04	17.9	17	47.38	17.15
1005	13	36.03	17.64	18	50.42	17.04
1006	15	42.02	17.38	19	53.33	16.93
1007	17	47.92	17.14	20	56.34	16.83
1008	19	54.09	16.89	21	59.36	16.67
1009	21	59.99	16.44	22	62.32	16.43
1010	23	65.9	16.21	23	65.38	16.26
1011	25	72.08	15.92	24	68.37	16.14
1012	27	78.12	15.69	25	71.35	15.97
1013	29	83.84	14.56	26	74.32	15.84
1014	31	90.04	13.17	27	77.38	15.71
1015	37	107.3	12.56	28	80.39	15.64
1016	39	113.57	13.22	29	83.37	14.89
1017	41	119.34	13.3	30	86.29	14.42
1018	45	131.06	14.21	31	89.28	13.9
1019	47	137.08	14.04	32	92.16	13.22
1020	49	143.09	14.02	33	95.07	12.97
1021	51	149.1	13.93	34	98.17	12.79
1022	53	155.12	13.77	35	101.26	12.63
1023	55	161.08	13.66	36	104.35	12.48
1024	57	167.18	13.49	37	107.31	12.49
1025	59	173.13	13.34	38	110.28	12.66
1026	61	179.17	13.22	39	113.24	12.85
1027	63	185.18	13.05	40	116.26	12.96
1028	65	191.16	12.81	41	119.13	12.97
1029	67	197.24	12.68	42	122.14	13.1
1030	69	203.22	12.51	43	125.27	13.13
1031	71	209.27	12.31	44	128.18	13.36
1032	73	215.28	12.11	45	131.17	13.54
1033	75	221.22	11.95	46	134.31	13.91
1034	77	227.2	11.72	47	137.24	13.96
1035	79	233.25	11.47	48	140.26	13.98
1036	81	239.17	11.26	49	143.24	13.93
1037	83	245.26	11.04	50	146.25	13.93
1038	85	251.24	10.89	51	149.2	13.85
1039	87	257.26	10.73	52	152.26	13.8
1040	89	263.29	10.56	53	155.29	13.74
1041	91	269.19	10.37	54	158.32	13.66
1042	93	275.18	10.24	55	161.32	13.61
1043	95	281.27	10	56	164.29	13.49
1044	97	287.25	9.74	57	167.47	13.42
1045	99	293.19	9.52	58	170.23	13.34
1046	101	299.16	9.31	59	173.25	13.27
1047	103	305.23	9.1	60	176.24	13.21
1048	105	311.18	8.88	61	179.23	13.14
1049	107	317.26	8.68	62	182.24	13.09
1050	109	323.23	8.44	63	185.24	12.97
1051	111	329.24	8.21	64	188.27	12.86
1052	113	335.27	7.98	65	191.25	12.78
1053	115	341.31	7.78	66	194.27	12.71
1054	117	347.37	7.53	67	197.28	12.64
1055	119	353.33	7.35	68	200.28	12.54
1056	121	359.36	7.19	69	203.26	12.47

1057	123	365.54	6.94
1058	125	371.38	6.75
1059	127	377.53	6.46
1060	129	383.4	5.38
1061	134	398.06	6.47
1062	136	404.09	6.29
1063	138	410.04	6.04
1064	140	416.01	5.92
1065	142	421.99	5.8
1066	144	427.98	5.68
1067	146	434.03	5.52
1068	148	440.12	5.42
1069	150	446.15	5.26
1070	152	452.15	5.12
1071	154	458.13	4.96
1072	156	464.07	4.76
1073	158	470.06	4.64
1074	160	476.09	4.42
1075	162	482.12	4.27
1076	164	488.12	4.07
1077	166	494.16	3.9
1078	168	500.13	3.72
1079	170	506.22	3.58
1080	172	512.2	3.45
1081	174	518.17	3.3
1082	176	524.15	3.11
1083	180	536.29	2.74
1084	182	542.23	2.54
1085	184	548.24	2.36
1086	186	554.27	2.19
1087	188	560.27	2.04
1088	190	566.18	1.92
1089	192	572.23	1.82
1090	194	578.12	1.69
1091	196	584.04	1.57
1092	198	590.31	1.4
1093	200	596.24	1.22
1094	202	602.29	1.04
1095	204	608.22	0.92
1096	206	614.29	0.79
1097	208	620.22	0.63
1098	210	626.09	0.55
1099	212	632.24	0.37
1100	214	638.26	0.16
1101	216	644.19	0

70	206.26	12.38
71	209.3	12.28
72	212.31	12.18
73	215.33	12.09
74	218.34	12.01
75	221.36	11.91
76	224.33	11.8
77	227.33	11.69
78	230.34	11.57
79	233.35	11.48
80	236.33	11.39
81	239.34	11.25
82	242.34	11.16
83	245.37	11.05
84	248.37	10.97
85	251.34	10.88
86	254.33	10.81
87	257.33	10.72
88	260.33	10.66
89	263.31	10.59
90	266.29	10.52
91	269.5	10.43
92	272.39	10.31
93	275.37	10.25
94	278.37	10.12
95	281.35	10.02
96	284.32	9.88
97	287.37	9.74
98	290.35	9.61
99	293.36	9.53
100	296.33	9.39
101	299.36	9.33
102	302.36	9.2
103	305.36	9.14
104	308.34	8.99
105	311.35	8.91
106	314.37	8.77
107	317.35	8.63
108	320.37	8.53
109	323.34	8.41
110	326.36	8.3
111	329.37	8.22
112	332.32	8.07
113	335.35	7.95
114	338.34	7.81
115	341.34	7.67
116	344.34	7.58
117	347.32	7.51
118	350.29	7.41
119	353.33	7.3
120	356.35	7.24
121	359.3	7.14
122	362.51	7.06
123	365.32	6.95
124	368.3	6.86
125	371.38	6.72
126	374.24	6.67
127	377.54	6.42
128	380.26	5.73
129	383.26	5.3
130	386.2	5.45

131	389.1	5.6
132	392	5.75
133	394.9	6
134	397.8	6.15
135	400.79	6.29
136	404.05	6.29
137	407.06	6.14
138	410.04	6.02
139	413.02	5.98
140	416.03	5.9
141	419.05	5.84
142	422.06	5.78
143	425.02	5.71
144	428.05	5.66
145	431.02	5.59
146	434.06	5.54
147	437.05	5.49
148	440.22	5.41
149	443.02	5.33
150	446.28	5.26
151	449.21	5.17
152	452.04	5.1
153	455.06	5.02
154	458.1	4.93
155	461.06	4.85
156	464.08	4.75
157	467.08	4.7
158	470.04	4.6
159	473.03	4.53
160	476.09	4.46
161	479.06	4.39
162	482.08	4.29
163	485.09	4.19
164	488.08	4.08
165	491.1	3.99
166	494.07	3.87
167	497.1	3.8
168	500.08	3.69
169	503.07	3.65
170	506.08	3.58
171	509.06	3.51
172	512.09	3.43
173	515.09	3.37
174	518.06	3.29
175	521.16	3.22
176	524.09	3.1
177	527.07	3.03
178	530.08	2.91
179	533.08	2.81
180	536.1	2.73
181	539.1	2.64
182	542.08	2.55
183	545.07	2.46
184	548.05	2.37
185	551.08	2.29
186	554.06	2.2
187	557.09	2.12
188	560.09	2.04
189	563.09	2
190	566.08	1.92
191	569.07	1.85

192	572.08	1.79
193	575.07	1.74
194	578.08	1.67

Test Well No.1. Formation Log.

Depth Range (m)	Stratigraphy and Description
0-4.87	Fine sand, some gravel and cobbles, brown, moist
4.87-5.18	Fine sand, some silt, brown, moist
5.18-8.23	Coarse sand, some fines, pebbles and granite boulders
8.23-10.97	Medium to coarse sand and fine gravel
10.97-14.02	Coarse sand with fine gravel
14.02-16.76	Fine gravel with coarse sand, caving at 55 feet.
16.76-19.81	Medium gravel turning to silty gravel, brown
19.81-25.91	Silty sand, brown
25.91-28.96	Silty fine sand, brown
28.96-33.83	Silty medium sand, brown
33.83-35.36	Silty medium to fine sand, brown
35.36-37.49	Silty medium sand, reddish brown
37.49-39.93	Silty medium to coarse sand, brown
39.93-40.84	Boulders, gravel and fine sand
40.84-44.20	Coarse sand with fines
44.20-58.52	Fine to coarse sand
58.52-67.66	Coarse sand with fines
67.66-76.50	Silty medium to coarse sand, brown
76.50-79.55	Silty medium to coarse sand, reddish brown
79.55-85.95	Silty medium to coarse sand, brown
85.95-98.15	Silty fine sand with some gravel, brown
98.15-101.19	Clay with sand and some gravel, brown
101.19-112.47	Silty sand, brown
112.47-118.57	Silty sand with cobbles, brown
118.57-133.20	Sandy clay with cobbles, brown
133.20-136.25	Sandy clay, reddish brown
136.25-141.12	Silty sand, yellow brown
141.12-144.17	Sandy clay, reddish brown
144.17-165.20	Silty sand and cobbles, brown
165.20-169.77	Silt with some sand, brown
169.77-172.82	Silt with some sand, cobbles and lime streaks, brown
172.82-179.83	Silty sand, gravel and some cobbles, brown
179.83-187.45	Silty sand,black metamorphic and quartz grains,brown
187.45-194.77	Silt with medium to fine sand, brown
194.77-195.38	Fine sand, brown
195.38-204.22	Silt with small amount of sand, brown
204.22-205.74	Silt with some sand, reddish brown
205.74-208.79	Silt with some sand, brown
208.79-217.93	Silty sand with some small gravel, brown
217.93-227.07	Silty sand, green-brown
227.07-230.12	Silt with some clay and sand, brown to green-brown
230.12-230.43	Medium brown clay
230.43-242.31	Silt with sand, green-brown
242.31-252.07	Silt with fine sand and some cobbles, green-brown
252.07-252.98	Clayey silt
252.98-257.56	Silt with fine sand and some cobbles, green-brown
257.56-260.60	Same as above with more rock

260.60-272.80	Silt with fine sand and some cobbles, green-brown
272.80-291.08	Silt with sand, light green-tan
291.08-306.32	Coarse sand, angular
306.32-307.85	Silt with sand, light green-brown

Appendix G
Test Well No.2. Formation Log

Depth Range (m)	Stratigraphy and Descriptions
0-12.19	Large rock and sand
12.19-25.91	Clay, silty sand and gravel
25.91-31.40	Smaill rock
31.40-71.02	Rock 2-4 inches
71.02-74.98	Brown sand mixed with black sand
74.98-75.29	Sand with some brown clay
75.29-153.31	Small rock witj 2-4 inches Rock
153.31-156.97	Brownish red clay with small rock
156.97-158.8	Hard rock
158.8-172.52	Soft cemented gravel
172.52-207.26	Small rock with some clay
207.26-241.40	Sand mixed with brown clay
241.40-247.80	Clay and rock-very hard
247.80-304.8	Sand and small rock-very hard